Interreg North Sea Region Jomopans

European Regional Development Fund

EUROPEAN UNION

Joint Monitoring Programme for Ambient Noise North Sea

2018 – 2021

Model predictions 2018 measurement sites

WP 4 - Deliverable/Task: T4.3

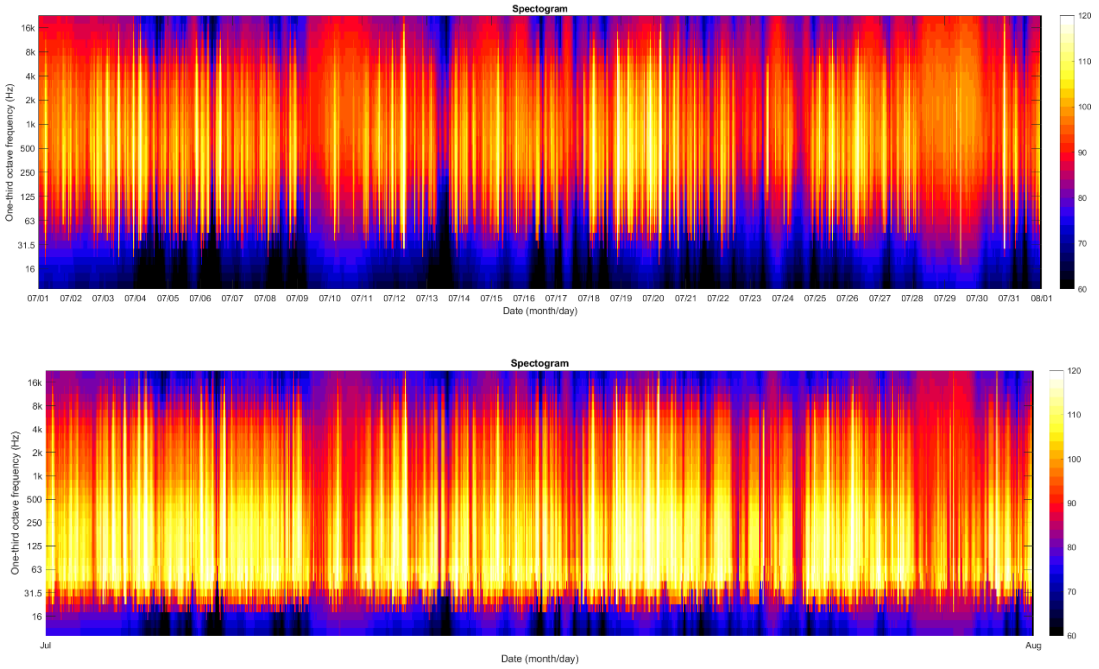

Authors: Bas Binnerts (TNO), Christ de Jong (TNO), Sander von Benda-Beckmann (TNO), Paul de Krom (TNO), Martin Östberg (FOI), Thomas Folegot (QO), Michael Ainslie (JASCO), Sam Welch (JASCO)

Affiliations: **TNO (NL), FOI (SE), QO and JASCO (for RWS, NL)**

Date: June 2021

Project Full Title	Joint Monitoring Programme for Ambient Noise North Sea
Project Acronym	Jomopans
Programme	Interreg North Region Programme
Programme Priority	Priority 3 Sustainable North Sea Region

Colophon	
First Author	Bas Binnerts
Organization Name	TNO
Email	bas.binnerts@tno.nl
Phone	+31 888663309

Version	Date	Review	Initial	Approval	Initial
001	July 2019				CdJ
002	Sept. 2019	Nathan Merchant	NM		CdJ
003	April 2021	WP4, WP5, WP6			BB

This report should be cited:
Binnerts, B, de Jong, CAF, von Benda-Beckmann, S, de Krom, P, Östberg, M, Folegot, T, Ainslie, MA, Welch, S (2020) *Model predictions 2018 measurement sites*. Report of the EU INTERREG Joint Monitoring Programme for Ambient Noise North Sea (Jomopans)

Cover picture: Predicted SPL spectrogram for UK Dowsing measurement location first and second iteration modelling (TNO)

Table of contents

Summary

The aim of the Jomopans project is to develop a framework for a fully operational joint monitoring programme for ambient noise in the North Sea. Output will be the tools necessary for managers, planners and other stakeholders to incorporate the effects of ambient noise in their assessment of the environmental status of the North Sea, and to evaluate measures to improve the environment.

Sounds are omnipresent in the underwater environment and can be produced by natural (currents, waves, weather, animals) and anthropogenic (shipping, construction) sources. International concern increasingly focusses on the potential negative effects of anthropogenic underwater noise on sensitive marine fauna. Sound sources, sound transmission, and the distributions of vulnerable species in the North Sea are all transnational questions which must be tackled transnationally, as specifically required by the Marine Strategy Framework Directive.

This report provides a description of the first and second iteration acoustic model calculations that are delivered to WP6 for validation against the experimental data from the 2018 monitoring stations. The observations made by WP6 described in [Putland et al, 2021] have been used to optimise the models, hence model updates are also described in this report.

1 Introduction

1.1 Introduction

The main objective of the modelling work package (WP4) is to develop and demonstrate verified and validated modelling methods applicable for generating maps of ambient noise in the North Sea, as input for assessment of the environmental status. Based on the guidance provided by WP3 (standardization) and experimental validation carried out by WP6 (validation), models are selected and implemented for the most predominant sound sources (ships and wind) and for underwater sound propagation in the North Sea.

To achieve this objective, the following tasks are carried out:

- T4.1: Initial selection of model inputs and outputs
- T4.2: Model verification and sensitivity studies
- T4.3: Model optimization (supported by experimental validation in WP6)
- T4.4: Sound maps
- T4.5: Modelling guidelines (together with WP3)

The T4.1 report [de Jong et al, 2018] provides an overview of the available models for sound sources (ships and wind) and sound propagation at the North Sea, and of the availability of input data. It includes a first assessment of the sources of uncertainties that come with the models.

The model implementation has been verified via benchmark scenarios in task 4.2. Different modelling methods have been tested and compared. The T4.2 report [de Jong et al, 2020] describes the results of the benchmarking and sensitivity studies for the acoustic models, leading to a selection of an appropriate modelling approach and providing insight in modelling requirements and quantitative uncertainties in model outputs.

Considering the modelling requirements defined in T4.2, the TNO model has been used to generate model predictions of the JOMOPANS acoustic metrics for selected time periods at specific monitoring locations at which the WP5 project partners have collected data in 2018. These model predictions have been compared against the measurements by WP6 [Farcas et al, 2021]. The observed differences provided guidance on how the modelling setup could be optimised. This T4.3 report describes the first and second iteration model predictions of sound level (from ships and wind) and a description of the model updates associated with the second iteration model results. Furthermore, the report describes a sensitivity study to better understand the modelling uncertainty.

In T4.4, the second iteration model configuration has been used to provide model predictions of the selected acoustic metrics [Merchant et al, 2018] for 2019 for the entire selected OSPAR North Sea region, for implementation in the management tools developed in WP7. The acoustic models will not be embedded in these tools, but all sound maps produced in WP4 are made available via the tool. These second iteration model predictions are evaluated by WP6 using the 2019 measurements and metadata from WP5 to quantify the uncertainty in the sound maps, see [Putland et al, 2021]. The calculated sound maps are reported in the T4.5 report [de Jong et al, 2021].

The WP4 T4.5 report [de Jong et al, 2021] informs readers about suggested modelling techniques and the associated uncertainty that have been applied for producing the sound maps of the North Sea region, provide advice and recommendations for modelling the main sources and propagation of underwater sound for similar applications, including a description of the most relevant sources of underwater sound, and sources of suitable input data.

1.2 Validation methodology

The acoustic modelling approach consists of modelling the source level of ships and of wind generated surface noise, as input to appropriate propagation models, that consider the effects of environmental properties (such as water depth and sediment type) on the propagation loss. Uncertainties in the predicted levels are associated with selection of the appropriate models and model settings as well as with the availability and quality of model input data. Random uncertainties in the model predictions can be incorporated in the statistical analysis (percentiles), while offsets in the model predictions can (ideally) be reduced by improving the model or the input data to the model.

The selection of acoustic models is carried out in a two-stage approach. Data from 2018 measurement sites have been compared (by WP6) against first iteration model predictions from WP4. Where necessary and possible, the modelling approach was updated, and revised predictions were provided to WP6 for the second iteration validation for the 2018 and 2019 sites. Figure 1 shows a schedule of the first and second iteration and proposed optimization methodology steps and tasks in the interaction

between WP4 and WP6. Note that within the JOMOPANS project no model data assimilation was done in the sense that the model results were not calibrated locally to minimize the model-data bias. The observed model data differences are used to decide on the required computational complexity and input of the selected model.

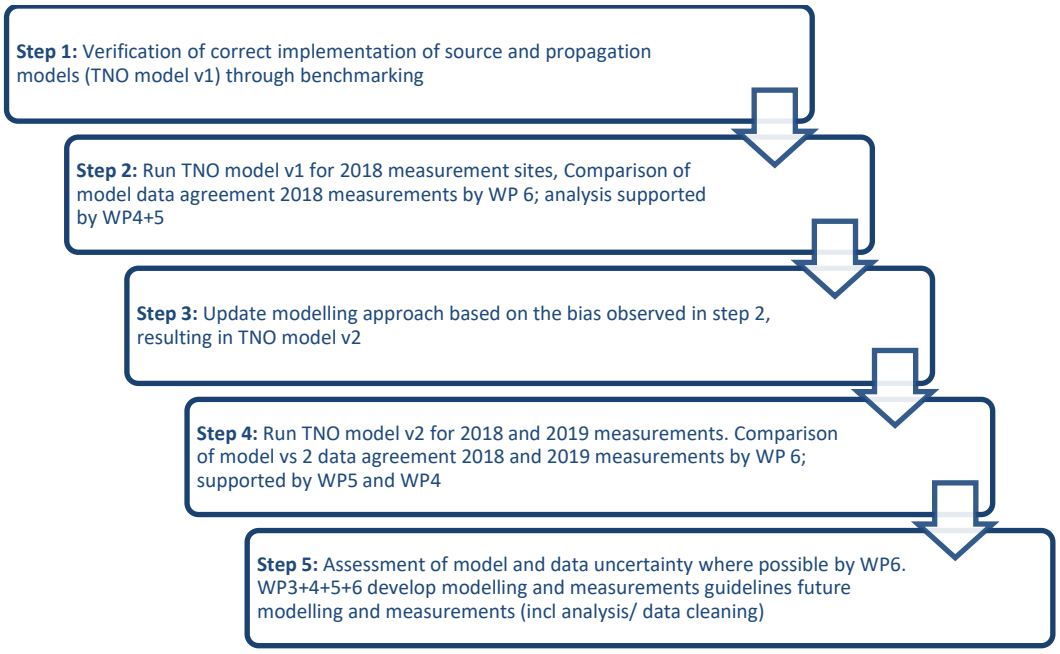

Figure 1 Overview of model validation and optimization steps adopted in the JOMOPANS project

The main focus of this report is on describing the modelling carried out by TNO, as the TNO model (v2) was used for generating the Jomopans sound maps in T4.4. Project partners FOI, Quiet Oceans and JASCO have actively contributed to this work by providing independent model predictions for selected sites with their models and model settings, and by contributing to the joint analysis of the results.

Analysis of the model-data differences provided insight in the uncertainties associated with the various assumptions in the modelling, as described in [Putland et al, 2021]. To understand possible causes of the remaining bias, TNO carried out additional modelling to study the effect of the environmental uncertainty and modelling method on the modelling uncertainty.

1.3 Measurement locations 2018

Acoustic data were acquired in 2018. The recordings of these systems were analysed in terms of time series of 1 s average SPL one-third octave band spectra and their monthly percentiles. The objective of these measurements (carried out in WP5) was to get experience with the offshore acoustic monitoring as well as to provide data for the acoustic model validation. A description of the measurements can be found in the WP5 measurement report.

Seven acoustic measurement stations were deployed in the Jomopans area during at least one month in 2018. In addition to the data of these seven sites, Norway provided one month of data from the Love station (site 8), with the aim to support the validation of wind noise models with data from a location with deep water and low shipping density. Figure 2 shows the eight measurement locations. Table 1 provides the coordinates of these locations, together with additional information about the measurement period and geometry and sediment. Due to technical problems, the sensor deployed at the German FINO1 site (3) did not record reliable data in 2018. Hence, data from this site are not included in this report.

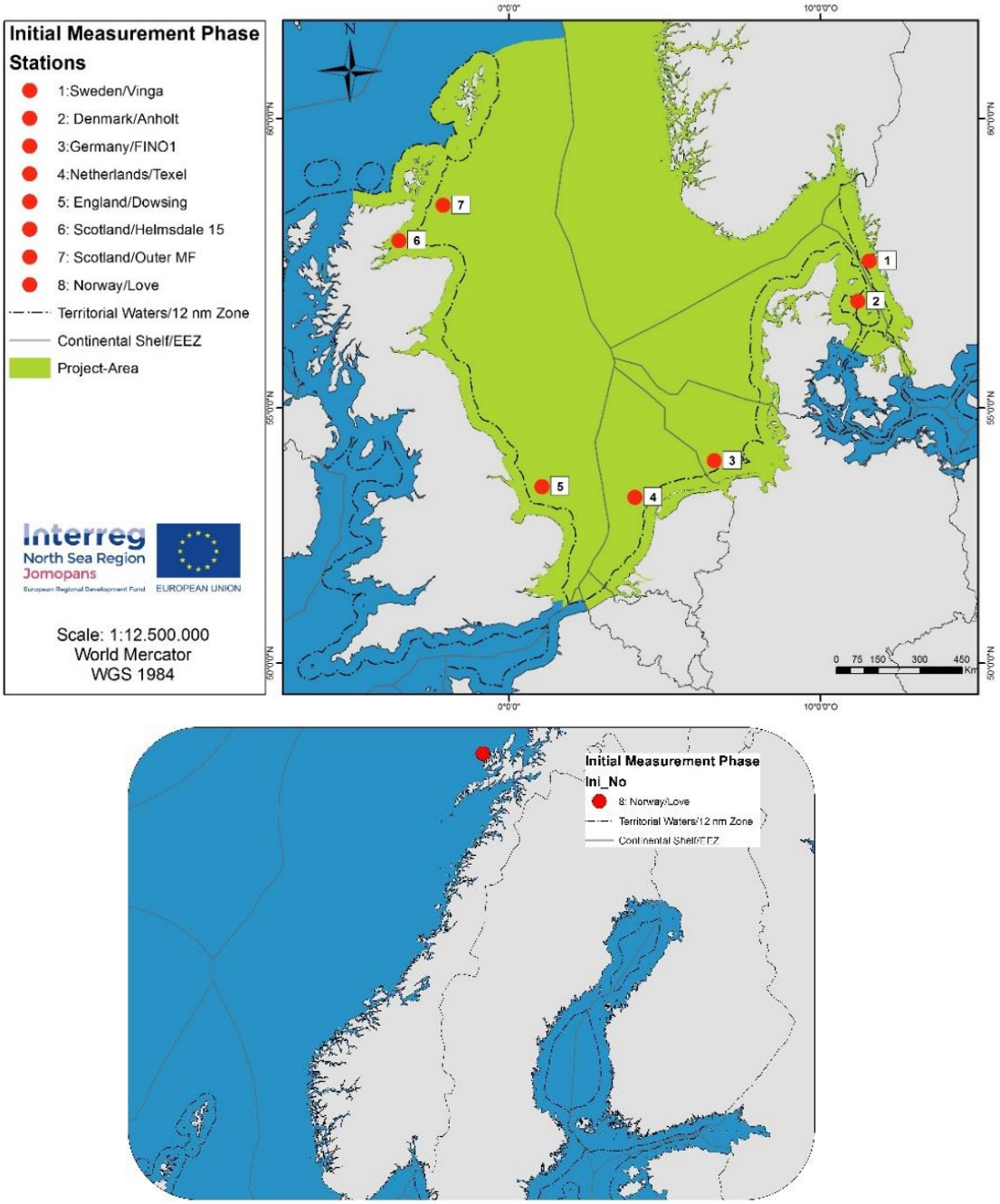

Figure 2 JOMOPANS 2018 measurement locations, indicated by red dots on the maps

Table 1: Jomopans 2018 measurement locations

	Station	Position (WGS84)	data period in 2018	Water depth	Sensor height above sea floor	Sea floor type
1	**Sweden_Vinga**	57.6272 N 11.5626 E	21 March–20 April	43 m	1.5 m	Mud
2	**Denmark_Anholt**	56.926667 N 11.2 E	July	10 m	3.0 m	Sand
3	**Germany_FINO1**	54.014861 N 6.587639 E	No useful data	30 m	1.5 m	Sand
4	**Netherlands_Texel**	53.316 N 4.043 E	15 October – 15 November	26.5 m	2.0 m	Sand
5	**England_Dowsing**	53.528597 N 1.05309 E	July	21 m	1.0 m	Sand
6	**Scotland_Helmsdale5**	58.05338 N -3.715252 E	May	48 m	3.0 m	Sand
7	**Scotland_MorayFirt**	58.57487 N -2.119471 E	May	23 m	3.0 m	Sand
8	**Norway_LoVe**	68.91 N 14.38 E	Apr	225 m	1.0 m	Sand

1.4 Terminology

Unless otherwise stated, acoustical terminology follows ISO 18405 and Wang and Robinson (2020).

2 Modelling methodology

2.1 Introduction

This section describes the various models and their configuration for the first and second iteration model predictions for the 2018 sites.

2.2 AIS data and processing

Quiet Oceans (QO) has delivered processed AIS data for 100 km × 100 km areas around the 2018 measurement stations for the selected months (Figure 3).

The processing carried out by Quiet Oceans involved:

1. Quality Check and Cleaning
   - Check the validity of the Maritime Mobile Service Identity (MMSI) vessel numbers from a static external database;
   - Check the validity of the length of the vessels by comparing with external databases;
   - Check the consistency of the date and time;
   - Check the consistency of the trajectory;
   - Check the consistency of the speed;
   - Remove non vessel data.
2. Trajectory interpolations to a regular temporal resolution of 1 minute

Figure 3 shows the 2018 data coverage as provided by Quiet Oceans. A detailed analysis of the AIS data for each measurement location in combination with the modelling results is provided in Annex A.

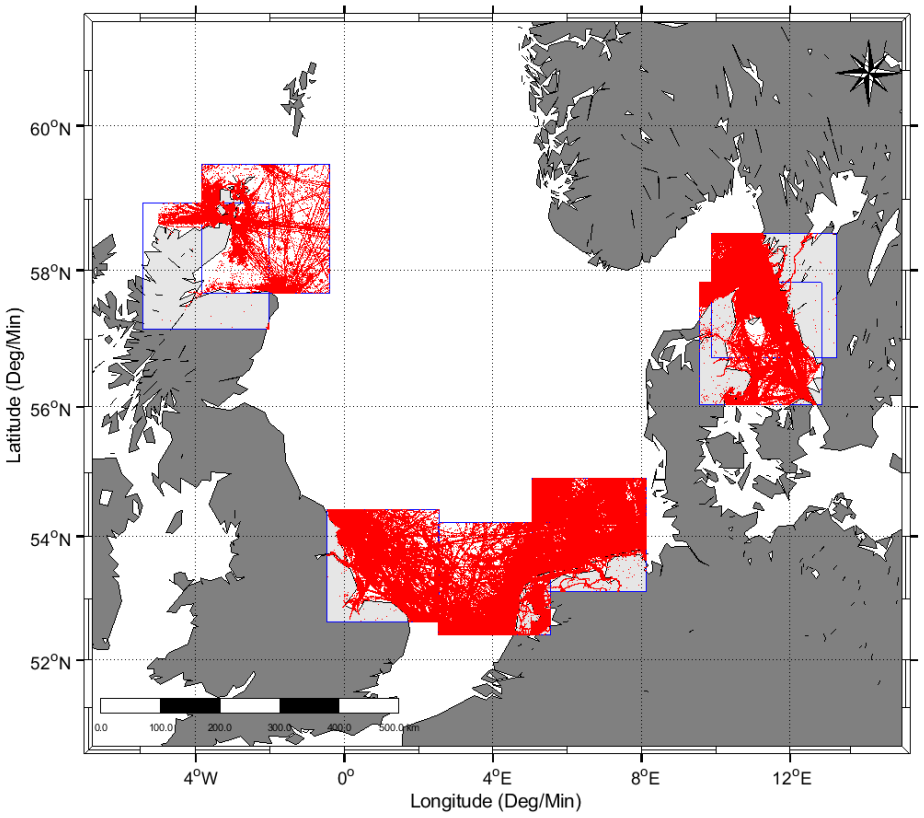

Figure 3 Image of Jomopans 2018 data provided by Quiet Oceans.

2.3 Ship source level model

The ship source level is calculated in the **first** and **second** iteration using updated versions of the RANDI 3.1 model [Breeding et al, 1996], that were developed in Jomopans on the basis of a large data set of measured ship source levels from the ECHO project [MacGillivray et al, 2019].

2.3.1 First iteration: RANDI3.1c model

The development of the **first iteration** model optimization, called RANDI3.1c, is described in the T4.2 report [de Jong et al, 2020]. The source depth for all ships is assumed to be fixed at 6 m below the water surface and the source location corresponds with the locations provided in the AIS data (without correction for the location of the AIS transponder on the ship). The RANDI 3.1c model calculates the ship source level spectrum (re 1 uPa^2 m^2/Hz), in one-third octave (base-10) bands, as a function of frequency (f), ship speed over ground (V), ship length (l) and ship type (vessel class, vc) :

$$L_S\,(f, V, L, \mathrm{vc}) = L_{S0}(f) + 60\log_{10}(V/V_{vc})\ \mathrm{dB} + 20\log_{10}(l/l_0)\ \mathrm{dB} + df \cdot dl + 3.0\ \mathrm{dB}, \quad (1)$$

where V_{vc} is a reference speed, $l_0 = 300$ ft is a fixed reference length, $dl = l^{1.15}/3643.0$ and

$$df = \begin{cases} 8.1\ \mathrm{dB} & \text{for } f < 28.4\ \mathrm{Hz} \\ 22.3\ \mathrm{dB} - 9.77\log_{10}(f/f_0)\ \mathrm{dB} & \text{for } 28.4\ \mathrm{Hz} < f \leq 191.6\ \mathrm{Hz} \end{cases} \quad (2)$$

where $f_0 = 1$ Hz.

The baseline spectrum $L_{S0}(f)$ is given by:

$$L_{S0,new}(f) = -10\log_{10}\left(10^{-A\log_{10}(f/f_0)-B} + 10^{C\log_{10}(f/f_0)-D}\right)\ \mathrm{dB} \quad (3)$$

with the fitted model parameters A, B, C, and D as given in Table 2.

The vessel class (vc) is obtained from the AIS 'ship type' parameter, according to Table 3, which also presents the fitted reference speed (V_{vc}) per vessel class. The maximum absolute value of the average difference (averaged over all vessel classes) in one-third octave bands between the RANDI 3.1c model predictions and the ECHO data is 2 dB, mean difference over the 20 Hz to 20 kHz bands is 1 dB and mean standard deviation of this difference is 6.5 dB. Hence, we assume that the statistical uncertainty in the predicted source level spectra is about 7 dB.

Table 2: Optimised baseline spectrum coefficients for the RANDI 3.1c source level model (Eq. 3), obtained by fitting coefficients of the RANDI 3.1 baseline model to ECHO residuals, see [de Jong et al, 2020].

Coefficient	A	B	C	D
Value	0.000	15.342	1.959	18.836

Table 3: ECHO vessel classes, based on AIS ship type ID, with fitted reference speed per vessel class for the first and second iteration source level models.

Vessel Class (vc)	AIS SHIPTYPE ID	Reference speed (V_{vc}) in knots	
		first	second
Fishing vessel	30	7.5	6.4
Tug	31,32,52	4.9	3.7
Naval vessel	35	14.2	11.1
Recreational vessel	36,37	14.0	10.6
Government/Research	51,53,55	9.2	8.0
Cruise vessel	60-68 (length $l > 100$ m)	20.2	17.1
Passenger vessel	60-68 (length $l \leq 100$ m)	11.7	9.7
Bulker	70, 75-79 (speed $V \leq 16$ kn)[1]	14.1	13.9
Container Ship	71-74 (all speeds) 70, 75-79 (speed $V > 16$ kn)	19.3	18.0
Vehicle Carrier	n/a	16.4	15.8
Tanker	80-89	13.1	12.4
Other	All other type IDs	8.8	7.4
Dredger	33	n/a	9.5

[1] 1 kn = 1852/3600 m/s

2.3.2 Second iteration: Jomopans-ECHO model

The **second** update of the ship source level model, called Jomopans-ECHO, is fitted to the same data set as the RANDI3.1c model:

$$L_S\,(f,V,L,vc) = L_{S0}(f) + 60\log_{10}(V/V_{vc})\ \text{dB} + 20\log_{10}(l/l_0)\ \text{dB}, \tag{4}$$

The baseline spectrum for all vessel classes is given by:

$$L_{S0}(\hat{f}) = K - 20\log_{10}(\hat{f}_1)\ dB - 10\log_{10}\left(\left(1-\frac{\hat{f}}{\hat{f}_1}\right)^2 + D^2\right)\ \text{dB}, \tag{5}$$

with $K = 191$ dB, $D = 3$ (for all classes, except $D_{\text{cruise vessel}} = 4$) and $\hat{f} = \frac{f}{f_{\text{ref}}}$, $\hat{f}_1 = 480\ \text{Hz}\ \left(\frac{V_{\text{ref}}}{V_{vc}}\right)$, $f_{\text{ref}} = 1$ Hz and $V_{\text{ref}} = 1$ kn.

For the cargo vessels (container ships, vehicle carriers, bulkers, tankers) the updated model includes an additional peak in the baseline spectrum below 100 Hz:

$$L_{S0,cargo}(\hat{f} < 100) = K^{LF} - 40\log_{10}(\hat{f}_1^{LF})\ \text{dB} + 10\ \log_{10}(\hat{f})\ dB - 10\log_{10}\left(\left(1-\left(\frac{\hat{f}}{\hat{f}_1^{LF}}\right)^2\right)^2 + (D^{LF})^2\right)\ \text{dB}, \tag{6}$$

with $K^{\text{LF}} = 208$ dB, $D^{\text{LF}} = 0.8$ (container ships and bulkers) or $D^{\text{LF}} = 1.0$ (vehicle carriers and tankers) and $\hat{f}_1^{\text{LF}} = 600\ \text{Hz}\ (V_{\text{ref}}/V_{vc})$.

NOTE: the above model expressions are for source spectral density level (Ainslie et al, 2020). In the final modelling these have been converted to source level in one-third octave bands by adding $10\log_{10}(0.231\,\hat{f})$ dB.

The source level model for dredgers is based on data from measurements by TNO in a project during the construction of Maasvlakte 2 (Rotterdam port extension). While dredging, the source level is much higher than would be predicted based on the speed, due to the propeller loading associated with the dredging. Based on the measurement results, the JOMOPANS-ECHO model prediction of the dredger source level at a sailing speed of 14 knots is applied as an estimation of the source level when the dredger is dredging (independent of the actual dredging speed). The AIS data available to Jomopans do not provide an indication when dredger is dredging, but it is tentatively assumed that a dredger is dredging when its speed is lower than 3 knots.

2.4 Ship propagation loss model

The propagation loss for the ship sources is calculated in the **first** and **second** iteration using TNO's **Aquarius 3** model, which combines a range-dependent analytical mode sum for the lower frequency bands with a flux integral model for the higher frequency bands. This model was verified against other models for the T4.2 benchmark test cases [de Jong et al, 2020].

A so-called '$N \times 2D$' approach is applied in which the range-dependent propagation loss is calculated along N radial trajectories from each ship source position. The parameters that were selected for these calculations, based on the sensitivity studies carried out in T4.2 [de Jong et al, 2020] and expert judgement of the WP4 partners, are summarized in Table 4.

Table 4: Aquarius 4 configuration parameters for first iteration model predictions for 2018 sites

Parameter	value
Number of radials (***N***)	16
Length of radials	min (100 km, distance to map edge)
Step size along radials	100 m
Source depth	6 m
Receiver depth	10 points, uniformly spaced from 1 m above sea floor to 1 m below sea surface

The environmental properties for the **first** (v1) and **second** (v2) iteration predictions for the 2018 measurement sites are modelled as follows:

2.4.1 Bathymetry

The water depth along the radials is obtained from linear interpolation from the available bathymetry input file to the discrete positions along the radials. The North Sea bathymetry is retrieved from the EMODnet data portal, with a resolution of 0.125º × 0.125º. The minimum water depth at which results are provided is 5 m. When the water depth along a trajectory is lower than 5 m, the trajectory is terminated, assuming that no propagation occurs beyond this point. Ship sources at water depths lower than 7 m are not considered, because of the assumed source depth of 6 m.

2.4.2 Water properties

Uniform properties of sea water are assumed: sound speed $1500\ \mathrm{m/s}$ and density $1000\ \mathrm{kg/m^3}$. Sound speed variations over the water column are tentatively ignored in this version of the model. Absorption in sea water (in dB/km) is implemented according to (Van Moll et al (2009)) in the second iteration. In the first iteration, the equation 2.2 from (Ainslie (2010)) was used, in alignment with the sensitivity studies described in the T4.2 report. The Van Moll model was expected to provide a more flexible estimation of the seawater attenuation as it allows the user to use North Sea typical parameters that determine the sea water attenuation. The parameters used are T=10 °C, S=34 ppt and pH_{NBS}=8

2.4.3 Water surface

In the **first iteration** the water surface is modelled as a perfect reflector for ship and wind noise, ignoring effects of surface loss due to wind and waves. In **the second iteration**, surface losses were included in the wind noise model predictions, but not in the ship noise model.

2.4.4 Seabed

The sea floor is modelled as a uniform acoustic 'fluid' per transect between source and receiver in both model iterations. The acoustic properties of the sediment (sound speed and absorption) are derived from sediment grain size data. For each source location. the sediment grain size is obtained via a linear interpolation of the median sediment grain size input file to the source grid location. Variations of sediment properties along the radial trajectories between source and receiver locations have been ignored, under the assumption that the variability has a limited effect on the modelling accuracy. A map of median grain size of North Sea surface sediments is retrieved from the World Data Center for Climate portal [Bockelmann, 2017]. These data do not include the areas around the Danish, Swedish and Norwegian measurement sites (1, 2 and 8). For these locations, the grain size parameter has been estimated on the basis of nearest neighbour extrapolation (site 1 and 2) and additional data.

In the **first version** of the modelling, the ratios of the compressional sound speed and the density of the sediment relative to those of the of the sea water at the see floor and absorption are derived from the grain size parameter ϕ from Table 4.18 in [Ainslie, 2010], applicable for the mid-frequency range (1-10 kHz).

In the **second version** of the modelling, a dispersive model for including frequency dependence of the sediment sound speed and attenuation was included to reduce the bias observed at lower frequencies between model predictions and data from measurements [Putland et al, 2021]. The following approach was followed to parametrize the seabed acoustical properties as a function of grainsize.

In the Aquarius 3 shipping noise modelling, the median grain size of the sediment at the source grid locations is obtained from linear interpolation of the data from [Bockelmann, 2017]. Variations of sediment properties along the radial trajectories from the source along which the propagation loss is calculated are tentatively ignored.

The acoustic properties of the equivalent 'fluid' sediment are derived from the median grain size, based on conversions provided in Ainslie [2010, section 4.4]. Table 4.17 from [Ainslie, 2010] gives the conversion for near-surface sediment properties, typically applicable in the frequency range 10 kHz to 100 kHz, and Table 4.18 for the bulk properties of the uppermost few metres of sediment, typically applicable in the frequency range 1 kHz to 10 kHz.

At lower frequencies (typically below 1 kHz) the sound penetrates deeper into the seabed, where sediment sound speed and density increase with increasing depth, and the absorption decreases. The increase can be gradual, but it can also exhibit sharp contrasts at transitions between sediment layers, particularly at rock layers that support shear waves as well as compression waves. Moreover, the propagation in porous sediment layers results in dispersion (frequency-dependent sound speed) and nonlinear dependence of attenuation and frequency (see e.g. [Kibblewhite ,1989]).

Appropriate information on the geoacoustic properties of the North Sea sediment layers in the frequency range relevant for shipping noise (typically 50 Hz to 1 kHz) is lacking. Moreover, the additional numerical complexity of a depth-dependent geoacoustic model is impractical for underwater sound mapping at North Sea scale. Therefore, the Aquarius modelling includes an approximation of the

seabed, modelled as a uniform 'fluid-like' half-space, with frequency-dependent acoustic properties.

The frequency dependence of the sediment properties is based on the 'low-frequency geoacoustic model for the effective properties of sandy seabottoms' published by Zhou et al [2009]. This model was developed from long-range acoustic measurements conducted at 20 shallow water locations in different coastal zones around the world.

Figure 2.4 shows the measured broadband sound speed ratio and attenuation from Zhou et al [2009].

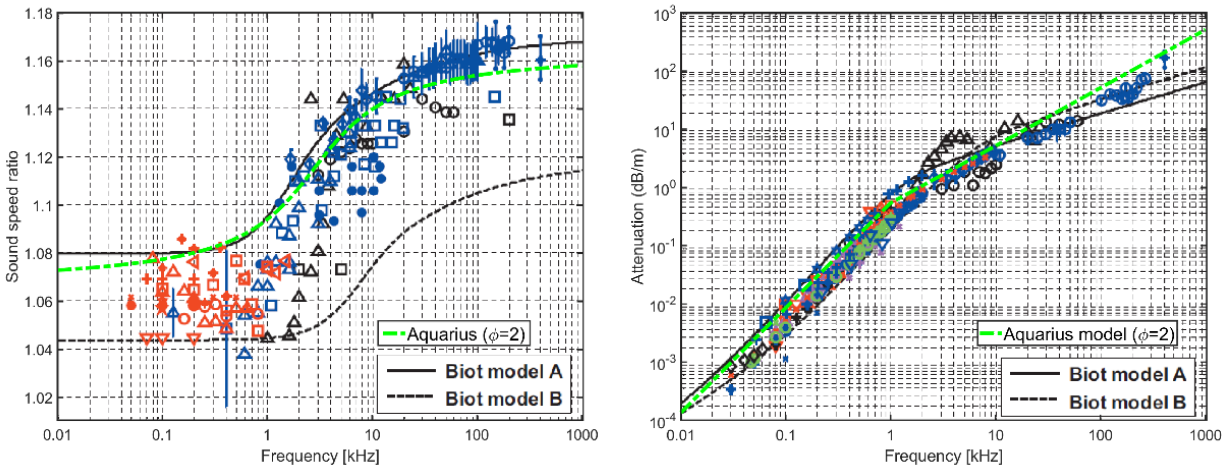

Figure 2.4 Measured broadband sound speed ratio (left) and attenuation (right) in sandy sea bottoms (Markers) compared with the Biot-Stoll model with the input parameters are adjusted to match either the sound speed ratio (Biot model A) or the attenuation (Biot model B), from [Zhou et al, 2009]. The green dashed lines give the results of the geoacoustic model implemented in Aquarius, for medium sand with a median grain size parameter $\phi = 2$.

The effective sound speed ratio c_r of the North Sea seabed applied in the Aquarius model consists of a parametrised inverse tangent curve:

$$c_r(f) = \text{atand}\left(a * \left(\log 10\left(\frac{f}{1\ \text{kHz}}\right) - b\right)\right) * c + d$$

where $\text{atand}(x)$ denotes the inverse tangent function with argument x in degrees.
This curve was fitted to the sound speed ratio data from [Zhou et al 2009]. As no digitised data was available, the fit was carried out to 5 data values selected "by eye" to roughly match the 'Biot model A' curve in Figure 2.4 (left): $c_r(10\ \text{Hz}) = 1.08$,): $c_r(100\ \text{Hz}) = 1.08$,): $c_r(1\ \text{kHz}) = 1.10$,): $c_r(10\ \text{kHz}) = 1.145$,): $c_r(10\ \text{Hz}) = 1.16$. Using the MATLAB curve fitting toolbox (nonlinear least-squares method) the parameters values were solved to be $a = 1.7778$, $b = 0.4508$, $c = 0.000554$ and $d = 1.1208$.

For the attenuation coefficient, the Aquarius model follows [Zhou et al 2009] by decreasing the absorption parameter in proportion with $f^{0.8}$, for frequencies below 1 kHz. The sediment density is a constant, independent of frequency, in alignment with [Zhou et al 2009].

Although the Zhou et al [2009] paper and data do not indicate a clear dependence on the median grain size, the Aquarius model was parametrized to include a grain size dependence, to match the tabulated geoacoustic parameters as a function of grain size for frequencies above 1 kHz, as provided in Ainslie [2010, section 4.4].

The sound speed ratio is adjusted by adding a constant value to the parametrised inverse tangent curve such that $c_r(10\ \text{kHz})$ is equal to the sound speed ratio $(c_{\text{HF}}(\phi)/c_w)$ from Table 4.17 [Ainslie, 2010]. To avoid a sound speed ratio smaller than 1, which is not supported by the Aquarius propagation model, the low-frequency part of the curve is limited to a fixed minimum value of 1.01. Though the sound speed ratio at the seabed surface can be lower than one, low-frequency sound penetrates deeper into the seabed, where sediment sound speed increases with increasing depth. The value 1.01 is selected as a tentative choice for implementing this effect. It is not supported by evidence or data, but it resulted in a good model-measurement agreement for the Vinga site [Putland et al, 2021]. There was < 6dB difference between model and measurement data for the 2019 data in the low frequency decade band 20 – 160 Hz. The model accounted showed close agreement despite seasonal thermoclines.

For the attenuation coefficient, the Aquarius model takes the value $\beta_{\text{HF}}(\phi)$ from Table 4.17 [Ainslie,

2010] for the frequency range above 1 kHz and calculates $\beta(f) = (f/1\ \mathrm{kHz})^{\,0.8}\beta_{\mathrm{HF}}(\phi)$ for frequencies below 1 kHz.

The frequency-dependent geoacoustic modelling that is implemented in the Aquarius model reduces the overestimation of low-frequency propagation loss that was observed in the first model-data comparisons [Putland et al, 2021], without direct fitting of the model to the North Sea shipping observations. Note, however, that model development was outside the scope of the Jomopans project and that the proposed geoacoustic model has not been further investigated or validated.

More accurate modelling of the underwater sound propagation in the North Sea at low frequencies would require more research and data acquisition, particularly in regions with a muddy seabed, such as the Kattegat.

2.5 Wind speed source and propagation model

2.5.1 Wind speed data

The Copernicus data set is used as the basis for the wind noise and sound propagation modelling, see the T4.1 report [de Jong et al, 2018]. We use the 10-minute averages of the U- and V-components of the wind speed vector measured at 10 m above the sea surface wind speed. The amplitude of the wind speed vector is computed as $v_{1\mathrm{h}} = \sqrt{v_U^2 + v_V^2}$.

This data set provides the selected wind data on a one-hour timescale and on a 0.25º × 0.25º spatial grid. This is linearly interpolated to the selected time resolution (10-minute) and to the Jomopans received grid (see Table 5) for the wind noise model predictions. Note that the 10-minute averaging time for the wind data is much longer than the 1-second averaging time that is specified for the acoustic metric. The implications of this difference have not been thoroughly investigated within the project. As discussed in section 2.5, a surface loss term was added to the associated propagation loss model.

The wind noise is calculated at the receiver grid locations (Table 5) as a function of depth (Table 4). The wind speed amplitude (at 10 m above the water surface) input for the wind noise calculations is obtained from linear interpolation from the available wind input file to the discrete grid positions and time steps.

Similar to the ship noise modelling, the **first** and **second** iteration wind noise predictions delivered to WP6 for validation are for the four nearest receiver grid locations around the measurement location and for the sensor location (through linear interpolation), both depth-averaged and at 1 m above the sea floor.

2.5.2 Wind noise model

The wind noise is calculated with the wind noise source and propagation models based on the semi-empirical expressions described in [Ainslie, 2010, Chapter 8], see [de Jong et al, 2018] and [de Jong et al, 2020]. The method used by the model is described by [Ainslie et al, 2011]. The propagation model is the same for both wind and rain, but only the wind source model was implemented in Aquarius. In the model wind is treated as a uniform sheet source, with a uniform source spectral density per unit area represented by the symbol K_f such that the areic dipole source spectral density level is $10\log_{10}\frac{K_f}{\mu\mathrm{Pa}^2\ \mathrm{Hz}^{-1}}$ dB. Alternatively, the sheet source could be represented by a large number of incoherently radiating point dipole sources at the sea surface, each with a dipole source spectral density level equal to $10\log_{10}\frac{K_f}{\mu\mathrm{Pa}^2\ \mathrm{Hz}^{-1}}$ dB $-10\log_{10}\frac{N}{\mathrm{m}^{-2}}$ dB, where N is the areic density of the point sources. The wind source level model uses Eq. 8.206 of [Ainslie, 2010] which gives K_f as a function of wind speed v at 10 m, frequency f, and air-sea temperature difference. If the water is warmer than air ($T_{\mathrm{air}} - T_{\mathrm{water}} < 1$°C) the model is independent of sea-air temperature difference, simplifying (for $v_{10} >$ 1 m/s) in these conditions to:

$$K_f = \frac{10^{4.12\left(\frac{v_{10}}{1\ \mathrm{m/s}}\right)^{2.24}}}{1.5+\left(\frac{f}{1\ \mathrm{kHz}}\right)^{1.59}}\ \mu\mathrm{Pa}^2\ \mathrm{Hz}^{-1} \tag{8}$$

This provides a smooth transition between the APL-UW (1994) wind noise source spectrum model, intended for the frequency range 10 kHz to 100 kHz, and the trend observed in measurement data from [Kuperman & Ferla, 1985] at lower frequencies, noting that the behaviour of the wind noise source level at frequencies of order 1 kHz and below is difficult to measure, and hence not well established. The quantity $10\log_{10}\frac{K_f}{\mu\mathrm{Pa}^2\ \mathrm{Hz}^{-1}}$ dB (wind areic dipole source spectrum level) is plotted as a function of

frequency in Figure 5.

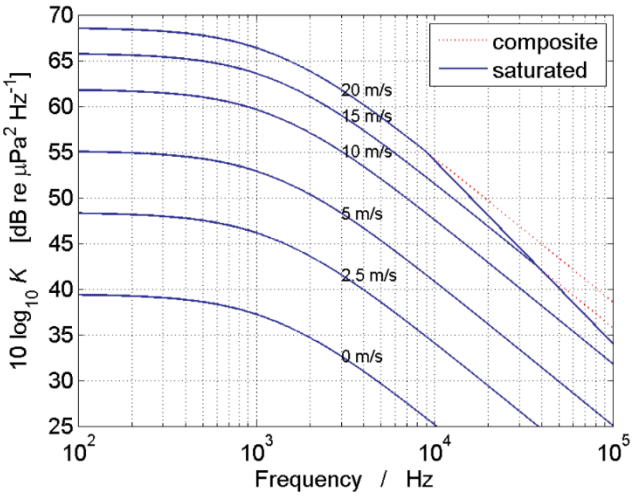

Figure 5 left Wind noise areic dipole source spectrum level versus frequency (figure 8.17 from [Ainslie, 2010]); ''composite''=evaluated using Equation (8.206); ''saturated''=composite model, capped using Equation (8.203)).

[Ainslie 2010, p.425]: At high frequency and sufficiently high wind speed (above about 30 kHz for a wind speed of 10 m/s, or above 10 kHz for 15 m/s) special attention needs to be given to the absorbing effect of near-surface bubbles. A pragmatic approach is to cap the dipole source level so that it does not exceed the following frequency-dependent value (obtained by inspection of Fig. 17 from [APL-UW, 1994, p. II-43]:

$$10\log_{10}(\pi K_{max}) = 79 - 20\log_{10}\left(\frac{f}{1\text{ kHz}}\right) \quad (9)$$

This saturation has not yet been implemented in Aquarius model.

In **the second iteration** surface losses were included for the wind model predictions to reduce the model overestimation observed in the comparison carried out in WP6. The wind model takes into account multiple reflections of surface noise via the seabed and sea surface, see section 5 of Ainslie et al. (2011).

The wind noise at depth d below the water surface is calculated as the sum of direct and reflected path contributions:

$$L_{p,f,wind} = 10\log_{10}\left(\frac{2\pi K_f(n_\mathrm{D}+n_\mathrm{BL})}{1\ \mu\mathrm{Pa}^2/\mathrm{Hz}}\right)\ \mathrm{dB} \quad (10)$$

with K_f the spectral density of the areic dipole source factor of wind noise [Eq 8.206, Ainslie, 2010]. and n_D and n_B the direct and reflected path contributions, see [Ainslie et al, 2011].

The direct path contribution is

$$n_\mathrm{D} = E_3(2\alpha d) \quad (11)$$

With α the attenuation coefficient of sea water and $E_3(x)$ is the exponential integral of third order, which can be approximated by Eq. 9.157 from [Ainslie, 2010]:

$$n_\mathrm{D} \approx \frac{e^{-2\alpha d}}{2\alpha d+3-e^{-0.434(2\alpha d)}} \quad (12)$$

At distances and frequencies where absorption can be neglected this approximates to $n_\mathrm{D} \approx 0.5$.

The absorption in water is currently estimated using eq.(2.2) from [Ainslie, 2010]:

$$\alpha = A_1\frac{F^2}{F^2+F_1^2} + A_2\frac{F^2}{F^2+F_2^2} + A_3F^2 \quad (13)$$

where F is frequency in kHz and:

$A_1 = 1.4\times10^{-2}$ Np km^{-1}, $F_1 = 1.15$ kHz,
$A_2 = 5.58$ Np km^{-1}, $F_2 = 75.6$ kHz, and $A_3 = 3.9\times10^{-5}\ Np\ km^{-1}$kHz^{-2}

These values are calculated from the empirical equations proposed by [Ainslie & McColm, 1998] for the representative temperature $T = 10$°C, salinity $S = 35$, depth $z = 0$ and acidity factor $K_\mathrm{pH} = 1$ (pH$_\mathrm{NBS}$ =

8), see [Ainslie, 2010, p.147].

The contribution of the reflected paths is

$$n_{\mathrm{B}} = \frac{1}{\eta}\left\{\sin\theta_c - (a-b)^{-1}\left[a^{3/2}\arctan\left(a^{-1/2}\sin\theta_c\right) - b^{3/2}\arctan\left(b^{-1/2}\sin\theta_c\right)\right]\right\} \quad (14)$$

with $a = 2\alpha H/\eta$ (for water depth H) and $b = 1/[2(kd)^2]$ (for wavenumber k).

The seabed and sea surface reflection losses are taken into account by means of an adjustment of the form $\eta = \eta_B + \eta_S$. Here η_{B} is the seabed reflection loss coefficient (see Eq. 8.86 of [Ainslie, 2010)], p.378):

$$\eta_B = 2w\epsilon\frac{cos^2\,\theta_c}{sin^3\;\theta_c} = 2w\epsilon\;\frac{v}{(v^2-1)^{3/2}} \quad (15)$$

This applies to coarse grained 'fluid' sediments with a sound speed ratio $v = c_{sed}/c_w > 1$, with critical angle $\theta_c = \arccos(1/v)$, density ratio $w = \rho_{sed}/\rho_w$ and attenuation parameter $\epsilon = \frac{\ln 10}{40\pi}\beta_{sed}$, with β_{sed} in decibel per wavelength. Note that the corresponding loss for fine sediments ($v < 1$) (see Eq. (8.86) of Ainslie (2010), p.378) has not (yet) been implemented. Surface loss η_S is calculated as a function of frequency and wind speed v_{10} (at 10 m above the sea surface) from a low-frequency sea surface reflection loss model, based on the measurements of [Weston and Ching, 1989] (Eq. 8.22 of [Ainslie, 2010, p.365], which is claimed to be valid up to an acoustic frequency of 4 kHz. The yearly averaged loss parameter is used.

$$\eta_S = 3.4\left(\frac{f}{1\ \mathrm{kHz}}\right)^{\frac{3}{2}}\left(\frac{v_{10}}{10\ \mathrm{m/s}}\right)^4 \quad (16)$$

At high frequency the effects of refraction become less important relative to those of absorption. This effect can be approximately taken into account by imposing an upper limit to the surface reflection loss of 15 dB at normal incidence (see Ainslie, 2010, p.368). This corresponds with $\eta_{S,\max} = 15\ln 10/20 \approx 1.7$. At a wind speed of 10 m/s, this limiting value would apply at frequencies above 637 Hz.
This upper limit is not implemented in Aquarius model.

2.6 Resolution and interpolation

Table 5 provides an overview of the parameters that determine the frequency, temporal and spatial resolution of the **first** and **second** iteration model predictions (TNO) for 2018 sites. For the final maps a 10 minute resolution was used. The underlying AIS data has a 1 minute resolution for the 2018 data.

Table 5: Modelling parameters for the first iteration model predictions for 2018 sites.

Parameter	value
Frequency bands	at the centre frequencies of the 20 Hz to 20 kHz one-third octave (base-10) bands
Time steps	Every 15 minutes
Receiver grid resolution	0.05 degrees longitude and 0.025 degrees latitude
Ship source grid resolution	the same resolution as the receiver grid, but shifted by one half of the grid resolution, with additional intermediate grid positions added ('fine grid' in Figure 6), see [de Jong et al, 2020]

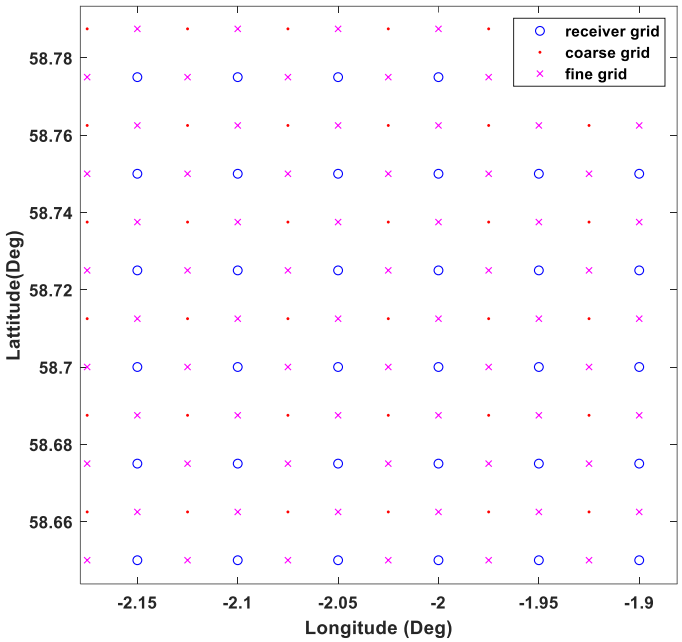

Figure 6 Example of the applied 'fine' source grid, along with the receiver grid

The results of the '$N \times 2D$' modelling are converted to a regular receiver grid through linear interpolation of the mean-square sound pressure spectra, both for the depth-averaged sound pressure and for the sound pressure at 1 m above the sea floor. The results at the sensor location are obtained via linear interpolation from the mean-square sound pressure at the four grid positions around that location. In the exceptional case where the SPL cannot be calculated at one or more of these grid positions, for example due to insufficient water depth (e.g. at the Scottish site number 6, see section 1.3), the results at the sensor location are taken from the nearest neighbouring grid location.

The **first** and **second** iteration model predictions delivered to WP6 for validation are for the sensor location and for the four nearest receiver grid locations around that location. The latter are added to provide insight in the spatial variability of the calculated metric and the uncertainties associated with the output grid resolution.

In order to increase the efficiency of the model calculations, the ship source locations, read from the AIS input file for each time step, are relocated to the nearest location on a predefined source grid [de Jong et al, 2020]. Hence, the propagation loss between the source and receiver grid positions can be calculated once and then stored. Next, for each time step, the propagation loss can be retrieved to be added to the ship source levels at the appropriate source positions for each time step.

2.7 Comparison of ship noise modelling methodologies

TNO provided first and second iteration model output for all 2018 measurement sites. In order to better understand the sensitivity of the model output to the modelling approach (i.e. model type and input), additional simulations were carried out by QO, FOI and TNO for ship noise modelling. Comparisons were made for the Texel and Vinga sites, because these have distinctly different sediment properties (Texel has a sandy seabed and Vinga has a muddy seabed). The set of tests was designed to provide insight in the following questions

1. What are the model differences when the input is nominally equal?
2. What is the effect of including a sound speed profile?
3. What is the effect of including surface loss?

Table 6 provides an overview of the "reference scenarios" that were designed to answer these questions. In addition to the table, more information is summarized below. The modelling results are shown in appendix B and the results are discussed in chapter 3. The results of the ship noise model runs are discussed in section 3.2.

1. **Tested propagation model:**
   - **TNO** used their **Aquarius** sound mapping framework and the **Aquarius 3** propagation model.
   - **Quiet Ocean** used their **Quonops** sound mapping framework, and a combination of their **RAM** and **Bellhop** based model implementations for the propagation modelling.
   - **FOI** carried out their modelling with the **RPRESS** Propagation model. Details on the models can be found in [De Jong et al, 2020].

2. **Modelled sites:**
   - **TNO** generated results for all 2018 measurement sites for both the first and second iterations model configuration (as described in this report).
   - **Quiet Oceans** generated modelling results for the Vinga, Texel, Dowsing and Moray Firth locations, where JASCO supported QO with the wind noise modelling.
   - **FOI** generated results for the Vinga site.
3. **Source model:**
   - **TNO** and **FOI** uses the Randi3C propagation model implementation
   - The **V1** QO ship noise model calculations use the original RANDI3 source level model [Breeding et al, 1978]
   - FOI uses the Randi3C propagation model implementation

4. **Bathymetry:**
   - **Quiet oceans** and **TNO** took into account the range dependent bathymetry for all model runs (using the bathymetric data from Emodnet available at 1/8 × 1/8 arc resolution).
   - **FOI** did not take into account the effect of the range dependency and used the water depth at the receiver.

5. **Model resolution:**
   - All model results presented are at 1m height from the seabed. The temporal resolution used is 15 min.

6. **Surface loss**
   - **TNO** and **FOI** do not take into account the surface loss.
   - **QO** takes into account a surface loss model from [Siderius et al, 2008].

7. **Seabed**
   - The TNO seabed modelling approach is detailed in section 2.4.4 of this report and in the T4.2 report [de Jong et al, 2020].
   - **QO** based its geology parameters on a conversion of geology folk classification data as described in [de Jong et al, 2020; chapter 5]), currently not taking into account dispersion.
   - **FOI** used the same parameters at the V1 of the TNO model.

8. **Water properties**
   - **TNO** does not take into account the sound speed profile stratification
   - **FOI** takes into account a constant depth dependent (but range and time independent) sound speed profile obtained from the Copernicus data portal. Figure 7Figure 7 shows the SSP used for the Vinga modelling.
   - **QO** takes into account a temporally and spatially varying SSP where the propagation losses are based on the time varying SSP (updated daily).

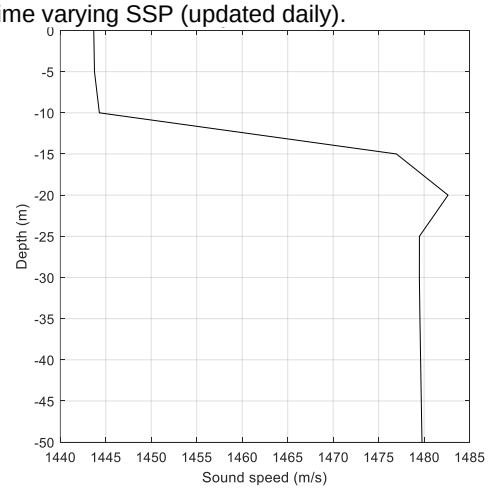

Figure 7: Monthly averaged sound speed profile used from the Copernicus data portal for the Vinga location. The strong stratification in the top layer is due to fresh water top layer typical for the Baltic sea.

Table 6 Tested modelling results. Note that for the Texel and Vinga sites, the TNO R11 results were generated for +- 1 & 2 ϕto understand the sensitivity of the model to a bias in the used grainsize.*

Partner	Ref	Loc.	Range dep. Bathy	Seabed	Water	Surface loss	Source model
TNO	R10	All	Yes	v1 (sec 2.4.4)	$c_w = 1500\ m/s$ $\rho_w = 1000\ kg/m^3$	No	Randi3.1c
TNO	R11*	All	Yes	v2 (sec 2.4.4)	$c_w = 1500\ m/s$ $\rho_w = 1000\ kg/m^3$	No	Randi3.1c
QO	R20	Vinga, Texel, Dowsing Moray Firth	yes	Folk based, ref	CMEMS profile	yes	Randi3
Controlled tests							
TNO	R12	Texel	Yes	$c_s = 1761\ m/s$ $\rho_s = 2014\ kg/m^3$ $\alpha_s = 0.88\ dB/\lambda$	$c_w = 1500\ m/s$ $\rho_w = 1000\ kg/m^3$	No	Randi3.1c
QO	R21						
TNO	R13	Vinga	Yes	$c_s = 1615\ m/s$ $\rho_s = 1702\ kg/m^3$ $\alpha_s = 1.22\ dB/\lambda$	$c_w = 1500\ m/s$ $\rho_w = 1000\ kg/m^3$	No	Randi3.1c
QO	R22						
QO	R23	Texel	Yes	$c_s = 1761\ m/s$ $\rho_s = 2014\ kg/m^3$ $\alpha_s = 0.88\ dB/\lambda$	$c_w = 1500\ m/s$ $\rho_w = 1000\ kg/m^3$	Yes	Randi3.1c
QO	R24	Texel	Yes	$c_s = 1761\ m/s$ $\rho_s = 2014\ kg/m^3$ $\alpha_s = 0.88\ dB/\lambda$	CMEMS profile	No	Randi3.1c
QO	R25	Vinga	Yes	$c_s = 1615\ m/s$ $\rho_s = 1702\ kg/m^3$ $\alpha_s = 1.22\ dB/\lambda$			
QO	R26	Vinga	Yes	$c_s = 1.077 \cdot c_w$ $\rho_s = 1.707 \cdot \rho_w$ $\alpha_s = 1.22\ dB/\lambda$			
FOI	R30	Vinga	No	$c_s = 1.077 \cdot c_w$ $\rho_s = 1.707 \cdot \rho_w$ $\alpha_s = 1.22\ dB/\lambda$	$c_w = 1500\ m/s$ $\rho_w = 1000\ kg/m^3$	No	Randi3.1c
FOI	R31	Vinga	No		CMEMS profile		

3 Modelling results

This chapter discusses the results of the **first** and **second** iteration model calculations for the noise from ships and wind at the 2018 measurement sites.

3.1 Analysis of model differences first and second iteration

The ship and wind noise modelling results have been delivered digitally to WP6, in 'hdf5'-files for the receiver depth and depth averaged (map values) at the exact receiver location (through interpolation based on the nearest C-square receiver grid positions. To verify the correctness of the modelling results (and model updates of the second iteration) and to support the analysis carried out in WP6 [Merchant, 2021], TNO generated various figures included in appendix A.

- Analysis of the AIS data
- cumulative distribution and histogram of the broadband SPL, at the sensor location and at the four C-square receiver grid positions surrounding that location.
- the spectral probability density of the SPL in one-third octave (base-10) bands.
- a time series of SPL one-third octave band spectra.

Figure 9 shows the probability spectral density of the modelled ship + wind noise at the Texel(top) and Vinga (bottom) measurement locations for the first (left) and second (right) iteration modelling. From these figures the effect of dispersion applied in the second iteration modelling is clearly visible (significantly increasing the modelled levels at lower frequencies). It is also observed that the effect is much more prominent for the sandy Texel site which is the consequence of the low sound speed ratio capped at a constant 1.01 (see section 2.4)

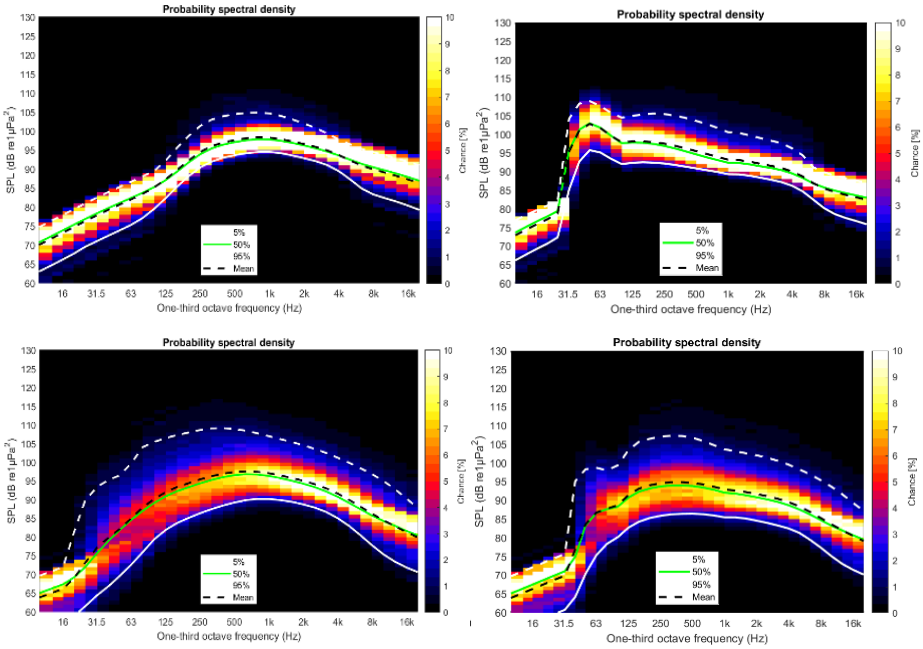

Figure 8: probability spectral density of the modelled ship + wind noise at the Texel(top) and Vinga (bottom) measurement locations for the first (left) and second (right) iteration modelling. The mean represents the geometric mean.

3.2 Wind noise model analysis

To investigate the added value of the wind noise model update, TNO together with WP6 carried out a detailed analysis of the modelled and measured wind noise levels. For this purpose, the 2018 JOMOPANS stations datasets were processed in WP6 to produce percentiles of the SPL over one month period, which were binned by wind speed category. In order to identify what model improvements were necessary for the wind noise model, the measurement data was binned in wind speed bins. The model results have been compared against two available datasets:

data v1 = 50th percentile of the SPL measured over one month, summarized in wind speed bins.
data v2 = 50th percentile of the SPL measured over one month, after removal of periods dominated by ship passages, using the ATL method (see Merchant et al, 2015] and [Farcas et al, 2020]), summarized in wind speed bins.

A qualitative visual inspection of the noise statistics suggested some wind speed categories, and frequency ranges likely did not represent actual wind noise, which were omitted from the analysis. The rationale is summarized in Table 7. The discarded sections were not considered in the development of the second iteration. Reasons for these were contributions from distance shipping, presence of flow noise, effects of low pass filters, and system noise (limiting measurements during low wind speed and higher frequencies in some cases).

Several model runs were carried out that predicted the 50th percentile for different wind speed categories:

- JOMOPANS-v1 = wind noise model without surface loss
- JOMOPANS-v2 = same wind noise model as JOMOPANS-v1, with wind driven surface losses added
- A deep-water version, which only included the contribution from the direct path (an extreme case that ignores multipath contributions; Eq. 8.206, assuming dT = 0, and Eq. 9.158 from Ainslie, 2010).

Finally, long-term measurements of wind noise on the LoVe station form 2014 (Ödegaard et al., UACE 2019) were also made available, which allowed to comparing wind noise level estimates in deeper waters and for a wider range of wind speeds and frequency. Contribution from shipping and transient events (e.g., marine mammals vocalizations) were removed using a running average filter (for details, see Ödegaard et al., 2019).

Table 7: estimated frequency range and wind speed categories in which measured 50% percentile $L_{p,ddec}$ is assumed to reflect wind-generated ambient noise for the 2018 sites.

	Station	Frequency range / Hz	Wind speed category / m/s
1	Sweden_Vinga	4000 - 12589	5 – 15
2	Denmark_Anholt	1000 - 12589	5 – 10
4	Netherlands_Texel	1995 - 20000	5 - 15
5	England_Dowsing	2000 - 12589	2.5 - 15
6	Scotland_Helmsdale	1584 - 6309	2.5 - 10
7	Scotland_MorayFirt	1258 - 6309	2.5 – 12.5
8	Norway_LoVe (2014)	10 - 20000	5 – 17.5

Figure 23 until Figure 25 show a comparison between the **first iteration** wind noise model against the 2018 measurements (processed in various ways). It is observed that the JOMOPANS-v1 wind noise model appears to significantly overpredict the wind noise levels for higher wind speeds (up to 12 dB, depending on site and frequency). A likely cause for the overprediction was the lack of surface-losses in the first iteration of the model, which would increase the absorption that will bring down the predicted wind noise levels.

Figure 26 - Figure 31 show a comparison of the JOMOPANS wind models (v1, v2 and deep-water expression) to the measured 50% percentile per site. As an extreme limit of surface loss, a deep-water propagation form for the wind-generated noise was considered (Eq. 8.206, assuming dT = 0, and Eq. 9.158 from Ainslie, 2010), which is appropriate for the high frequency (> 1 kHz) comparison done here. The JOMOPANS v2 predictions were closer to the measured wind noise levels, although there still appeared to be an overestimation by the v2 model. The deep-water expression tended to provide a closer match with the measured wind noise levels.

Figure 32 and Figure 33: the data from the LoVe station (Ödegaard et al., UACE 2019) in 2014 LoVe (Site 8) provided data over a longer timeframe for a wider range of wind speeds, and deeper water environments. Bottom conditions were found to be variable around the LoVe station, so we considered a range between medium sand ($\phi = 1.5$) and medium silt ($\phi = 5.5$) for the seafloor properties. At low frequencies (< 1 kHz) the JOMOPANS v2 model predictions were consistent with the measured noise levels at low wind speeds, especially when considering the medium sand scenario. However, for higher wind speeds, (> 10 m/s) a low frequency bump was not predicted by the model. At higher frequencies (> 1 kHz) , the levels around frequencies with maximum ddec band energy peak were well predicted by the JOMOPANS v2 model, but the slope at higher wind speeds appears to steeper than predicted by the model. It is unclear what the cause is. A potential explanation is the lack saturation effects, although available data suggest this should have limited effect. Alternatively, the absorption model may underestimate the amount of absorption, which would increase the slope of the wind noise levels with increasing frequencies. Uncertainties in seafloor properties are unlikely to explain the lack of match, since the deep-water expression (containing only the direct-path contribution) also predicts a similar fall-off. In summary, the LoVe data analysis indicates that at

- low frequencies: matches well at low wind speeds, but the low frequency bump at higher wind speeds was not predicted by the model.
- at higher frequencies: levels around frequencies with maximum ddec band energy peak well predicted, but slope at higher wind speeds appears to steeper than predicted by the model.

3.3 Analysis of model differences between scenarios

To better understand the sensitivity of the modelling results to the various model input parameters and modelling methods used by the WP partners, FOI, QO and JASCO carried out additional model runs of which details can be found in section 2.7. The resulting figures are included in appendix B. In this section, the Texel and Vinga modelling results are analysed in more detail. Figure 9 shows the 50th percentile of the modelled and measured one-third octave band sound pressure level spectra for the Vinga and Texel sites (Other percentile plots can be found in appendix B). For the TNO model, results are shown for a spread of grainsize values (ϕ ±1 and ±2) in order to illustrate the effect of a bias in the seabed grainsize data (assuming the method for converting the grainsize to acoustic properties is correct). It should be noted however that the uncertainty of the grainsize data is not known, implying that these results can only be used to illustrate the parameters sensitivity, not to properly evaluate the expected modelling uncertainty.

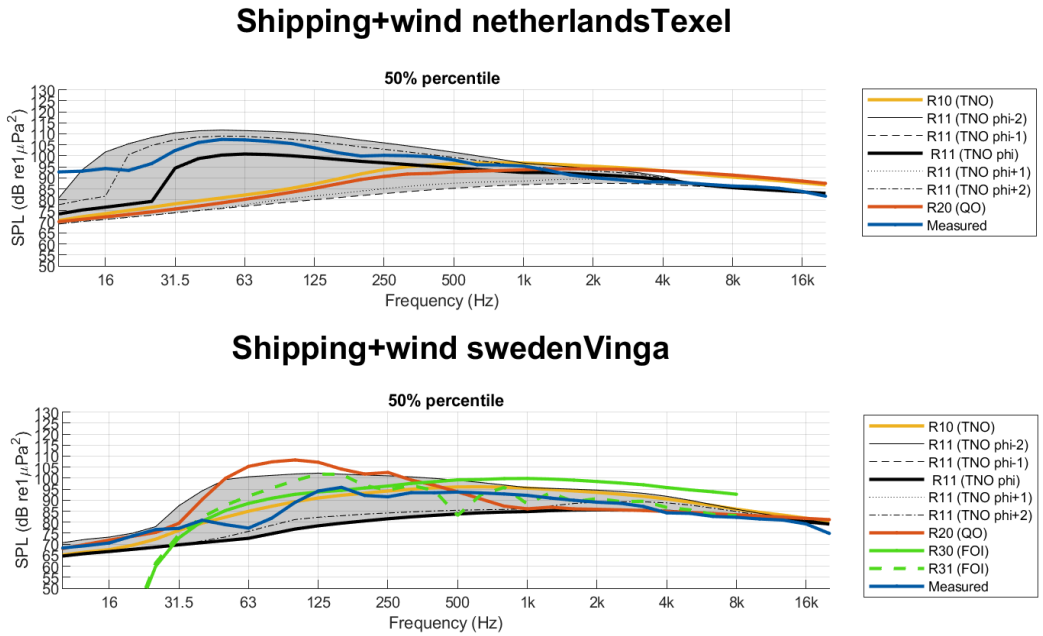

Figure 9: Modelled levels for the Vinga (top) and Texel (bottom) sites, with the second iteration model configuration (TNO), default operational settings (QO), and a variation of settings for FOI

The spread in the results presented in Figure 9 suggests that the differences in model input used by the partners have a significant influence on the model outcome (much more than the choice of the propagation model). Comparing for example the default mode of operation of QO (R20) with the V1 (R10) and V2(R11) results of TNO shows differences up 20 dB for specific decidecade band levels. It can however not be concluded from this set of results what aspects of the modelling approach have the biggest influences on model output. To better understand the cause of the observed differences, various additional simulations were carried out (as described in section 2.7). Figure 10 shows the median levels for the selected additional “reference” model runs for ship noise. Results for the other percentiles are included in appendix B.

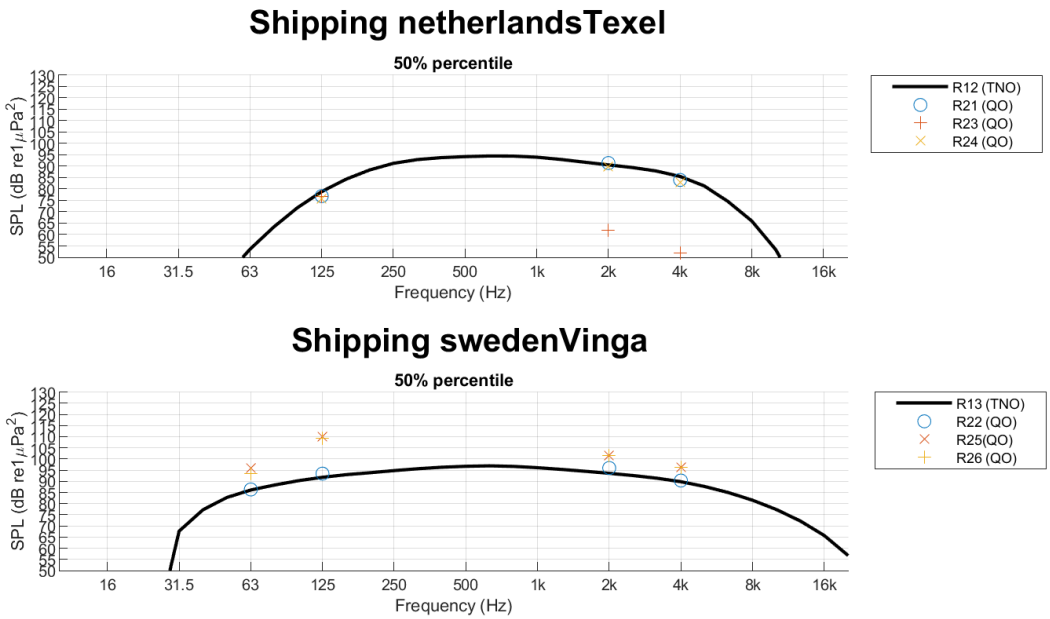

Figure 10: Modelled levels for the Vinga (top) and Texel (sites), with the reference model configuration described in section 2.7

Based on the results presented in Figure 9 and Figure 10 (and the complete set of results for all percentiles in appendix B), the following observations are made regarding the specific modelling aspects.

Propagation and mapping: TNO, QO and FOI use different propagation models, but it was concluded from the task 4.2 benchmark studies that the differences between these models, for the same input parameters was limited to a few dB (de Jong et al, 2020). This observation is confirmed by the Vinga **(R13 (TNO) & R31(QO))** and Texel **(R12 (TNO) & R21(QO))** results**.** These results also suggest that other differences in "sound mapping parameters" (number of radials, spatial interpolation, time and spatial resolution and source gridding) have a limited influence on the model differences.

Seabed acoustic values: The TNO, QO and FOI model predictions are based on substantially different sediment parameters. In the second iteration TNO modelling (Figure 9) the effect of seabed dispersion was taken into account. This dispersion effect is observed to result in in significantly higher levels at lower frequency for the Texel site (with respect to the first iteration TNO model results and the partner contributions). Furthermore, the uncertainty bounds presented in Figure 9 (**R11(TNO)**) suggest that an uncertainty in the grainsize is likely to be a major factor driving the uncertainty, which may also explain the large spread in inverted seabed acoustical parameters observed in [Zhou et al 2009] (section 2.4). The measurement data plotted in Figure 9 suggest that taking into account frequency dependent properties for the seabed significantly reduces the bias observed the measurements.

Sound speed profile: The sound speed profile effectively results in a focussing of acoustic energy towards the direction (upwards or downwards) where the sound speed decreases. A positive gradient results in more interaction with the ocean surface which effectively leads to higher losses due to surface induced scattering and attenuation but less interaction with the seabed. A negative gradient effectively results in the opposite effect.

In well mixed shallow water however (typical for the North Sea region), the amount of stratification is limited, hence it is expected that the effect of the sound speed profile is less important than e.g. in deep water where sound is channelled in ducts, strongly affecting the sound propagation. To investigate the effect of the sound speed profile (SSP), QO modelled the sound levels for Vinga **(R25 & R26)** and Texel **(ref 24)**, keeping the other input parameters constant. The **R26** case uses a constant ratio of the sound speed ratio at the water seabed interface, which is expected to be a physically more correct way of modelling the geo-acoustic parameters for the water sand mixture of the upper seabed layers. QO also provide similar calculations for the Vinga site, but neglecting the range dependence of the SSP and the bathymetry **(R30 & R31)**. The results indicate that for the Texel site the effect of the sound speed profile is small (a few dB) except at the lowest tested frequency (63 Hz) where a small change in the angle of incidence with the seabed is expected to have resulted in ~7 dB increased loss. For the

Vinga site, the inclusion of an SSP however leads to significantly higher levels for the QO and FOI modelling results (Figure 10). This is attributed to upward refraction caused by the sweet water top layer, which reduces the acoustic propagation losses due the interaction of the sound with the seabed. The strong stratification in the top layer is typical for the Baltic Sea, and hence may be an important factor to take into account in the JOMOPANS region east of Denmark. The model data comparison described in (Putland et al, 2021) did however not clearly confirm the need for modelling the time varying SSP.

Surface loss: The QO model predictions include the effects of surface loss (driven by waves). The TNO and FOI predictions ignore this effect for the ship noise modelling. The **(R23)** variation shows the impact of including this effect at 63 Hz, 125 Hz, 2 kHz and 4 kHz. The effect of the surface loss results in significantly lower ship noise levels at high frequencies.

Range dependence: Range dependence of parameters can become relevant in case there is significant spatial variability in the bathymetry, geology and ocean parameters. TNO takes into account range dependence of the bathymetry directly in the model, but assumes that the seabed parameters are relatively homogenous over the area where a ship contributes, approximating the grainsize along all radial transects by the grainsize at the source grid cell. QO takes into account range dependence of the bathymetry, SSP, surface los and seabed acoustical parameters. FOI did not include any range dependence in the modelling for Vinga, and assumed the water depth to be equal to the depth at the receiver. A comparison of the FOI SSP results **(R30 & R31)** with the QO results **(R25 & R26)** for Vinga (Figure 9) suggests that the effect of taking into account the bathymetry may be a less important factor than the combination of taking into account the SSP and proper seabed acoustical parameters for the Vinga site.

Ship source level model: As described in section 2.3 and section 2.7; different source models were used in the different iterations and runs. No dedicated simulation was however carried out to understand the impact of the source level choice on the modelling results (keeping the other parameters constant).

4 Conclusions and way ahead

This report describes the first and second iteration model predictions and the model updates associated with the second iteration model results. It is important to note that the 2018 measurements were not used to calibrate the model. No attempt was made to introduce correction factors in the model to reduce the observed model-measurement bias and uncertainty. The rationale behind this is that local optimization of the model can lead to a false sense of confidence in the model accuracy on a larger North Sea basin scale when not enough data points are used to allow for an independent validation.

Instead, the selected three main updates in the second iteration of the modelling approach were based on suggestions from independent data sets.

- Optimization of the semi-empirical ship source level model, using data from the ECHO programme of the Port of Vancouver and Transport Canada.
- Optimization of the semi-empirical sea floor geo-acoustic model, based on the dispersion curves presented in [Zhou et al, 2009]
- Optimization of the semi-empirical wind noise model [Ainslie et al, 2011]

These were selected after the first model- measurement comparison, and address the main trends in the observed model- measurement deviations. In particular, the update of the sea floor geoacoustic model was aimed at reducing the observed underestimation of the low frequency ship noise levels in the areas with a sandy seabed.

In a future ideal scenario, uncertainties in the modelling input and model subcomponents are well understood such that any uncertainty in the model input can be forward propagated to provide a confidence assessment of the produced map levels; which would be supported by data that would lie within the modelled uncertainty bounds. The current state of the art modelling is however not yet able to provide this assessment because uncertainty in the modelling input is not well understood.

To support the formation of hypotheses on the main factors that drive the observed model measurement differences discussed in WP6 [Putland et al, 2021] and to provide guidance on the importance of the different aspects of modelling, the WP4 partners ran additional simulations for selected sites (section 3.2). The comparison of the default models and input parameters used by TNO, QO and FOI showed significant differences in the predicted ship noise levels. To understand these differences, various additional results were generated to understand the cause of the differences. These insights, in combination with the model measurement comparison described in [Putland et al, 2021], form the foundation of the modelling guidelines report [de Jong et al, 2021].

Below, the contribution of the various modelling components to the model uncertainty is discussed per sub-element of the modelling.

JOMOPANS-ECHO source level model: The underlying echo data set suggests a 6 dB uncertainty in the prediction of individual ship source levels. The analysis shown in [de Jong et al, 2021] suggest that the uncertainty in the individual ship source levels has only a limited influence on the predicted monthly SPL percentiles.

Wind noise model (Annex C): Due to potential contribution of sources other than wind generated noise (distant shipping, flow noise, low-pass filters, electronic noise floor), and differences in averaging time, it was challenging to compare the 2018 summary statistics to model predictions. Nevertheless, the JOMOPANS-v2 wind noise model appears to improve predicted wind noise levels compared to v1 (smaller difference with observed median wind noise levels) for higher wind speeds. Changes in predicted wind noise levels could be up to 12 dB, depending on site and frequency. The main improvement was a consequence of the inclusion of surface losses in the second iteration. The roll-off of te wind nose spectra at higher frequency, especially for higher wind speeds, is steeper than predicted with current models. This is reminiscent of saturation effects (see Eq. 8.203 in Ainslie, 2010), but one expects that this would start to only have an effect for wind speeds > 15 m/s. Possibly this mechanism is exacerbated in shallow waters. Alternatively, this roll-off is better matched using models that predict more high frequency attenuation. At some locations the spectra look ‘bumpy’, which could be due to small number statistics, or possibly rain that is not included in model. To make further progress time series need to be compared in more detail at a comparable averaging time as the wind noise measurements. This allows for more insight to determine the dominating noise source was and therefore more effective filtering.

Sound speed profile: It was observed that including the effects of a sound speed profile in the propagation loss modelling led to a significant increase in modelled levels for the Vinga area, which is characterised by a muddy seabed and strong stratification. For the Texel site, with a sandy seabed, the

effect of the SSP was small. These observations suggest that the effect of the SSP may be relevant in regions with a muddy seabed, at low frequencies, where a small change in the angle at which sound interacts with the seabed has a large impact on the reflection of sound. The analysis shown in [Sertlek et al, 2016] confirms that the effect of the sound speed profile is small in regions where the seabed is predominantly sandy.

Seabed model: The strong sensitivity to the sediment parameters and the effect of dispersion observed at low frequencies suggest that the geoacoustic model of the seabed is the main factor that drives the model uncertainty at lower frequencies where the ship noise dominates the soundscape. For the second iteration modelling, TNO selected a geoacoustic model based on the measurements summarized by [Zhou et al 2009]. The applicability of this model for the North Sea sediments is uncertain, and the extrapolation of the model to muddier seabed (such as typical for the Vinga area), requires further validation. Up to this point, the JOMOPANS data could not be used to calibrate the geoacoustic model because all data were designated for the evaluation of the model-measurement agreement by WP6. It is recommended to further investigate if the geoacoustic properties around the different measurement sites shows a correlation with the observed model-measurement differences.

Surface loss: The effect of the surface loss becomes increasingly important at higher frequencies and wind speeds. Though the wind model predictions could benefit from taking into account the effect of the surface loss, it remains unclear if there is a need for including the surface loss for ship noise modelling. Comparison of the TNO and QO modelling results show that the inclusion of the surface loss (QO results) can have a significant effect on the model output. The effect of the surface loss on ship noise modelling is not included by TNO, because taking into account surface loss effects on the sound propagation results in a significant increase of computation time as propagation losses need to be computed for multiple wind speeds. The added value of this increased computational complexity was considered insufficient given the lack of data supporting its importance.

Bathymetry: the model predictions are not very sensitive to uncertainty in the exact bathymetry. An exception may be in very shallow water at frequencies below or near the waveguide cut off frequency. This may be an issue in coastal shallow water with high tidal variability at low frequencies. Because of the low trust in very shallow water propagation loss modelling, no sound levels were included in the maps at depths smaller than 5 m. Tidal variations have not been taken in account in the TNO modelling.

References

Ainslie, 1995	M.A. Ainslie, "Plane-wave reflection and transmission coefficients for a three-layers elastic medium", JASA 97 (2), 1995, pp. 954-961, extended to various layers
Ainslie & McColm, 1998	Ainslie, M.A. and McColm, J.G. (1998) A simplified formula for viscous and chemical absorption in sea water. J. Acoust. Soc. Am. 103 (3), 1871-1872
Ainslie, 2010	Ainslie, M.A. (2010). *Principles of Sonar Performance Modeling*. Springer
Ainslie et al, 2011	Ainslie, M.A., Harrison, C.H. and Zampolli M. (2011) An analytical solution for signal, background and signal to background ratio for a low frequency active sonar in a Pekeris waveguide satisfying Lambert's rule. Proc. 4th International Conference and Exhibition on "Underwater Acoustic Measurements: Technologies & Results"
Ainslie et al, 2020	Ainslie, M.A., C.A.F. de Jong, S.B. Martin, J.L. Miksis-Olds, J.D. Warren, K.D. Heaney, C.A. Hillis, and A.O. MacGillivray. 2020. ADEON Project Dictionary: Terminology Standard. Document 02075, Version 1.0. Technical report by JASCO Applied Sciences for ADEON. https://doi.org/10.6084/m9.figshare.12436199.v2
APL-UW, 1994	APL-UW (1994) High-Frequency Ocean Environmental Acoustic Models Handbook. *Applied Physics Laboratory, University of Washington, APL-UW TR* 9407
Bockelmann, 2017	Bockelmann, Frank-Detlef **(2017)**. *Median grain size of North Sea surface sediments*. World Data Center for Climate (WDCC) at DKRZ. https://doi.org/10.1594/WDCC/coastMap_Substrate_MGS
de Jong et al, 2018	de Jong, C.A.F., Binnerts, B., Östberg, M., Folegot, T., Ainslie, M.A. (2018) *Jomopans model and data inventory*. Report of the EU INTERREG Joint Monitoring Programme for Ambient Noise North Sea (Jomopans).
de Jong et al, 2019	de Jong, C., Binnerts, B., Prior M., Colin. M, Ainslie, M., Mulder, M, Hartstra, I. (2019), TNO report *Wozep – WP2: update of the Aquarius models for marine pile driving sound predictions*
de Jong et al, 2020	de Jong, C.A.F., Binnerts, B., Östberg, M., Folegot, T., Ainslie, M.A. (2018) *Jomopans model benchmarking and sensitivity studies*. Report of the EU INTERREG Joint Monitoring Programme for Ambient Noise North Sea (Jomopans).
de Jong et al, 2021	de Jong, CAF, Binnerts, B, Robinson, S, Wang, L (2021) Guidelines for modelling ocean ambient noise. Report of the EU INTERREG Joint Monitoring Programme for Ambient Noise North Sea (JOMOPANS).
Farcas et al, 2020	Farcas, A., Merchant, N.D. (2020) Uncertainty assessment between measurements and model predictions for 1st and 2nd iteration 2018 data. Report of the EU INTERREG Joint Monitoring Programme for Ambient Noise North Sea (Jomopans).
Fugro, 2017	Geophysical Site Investigation Survey, Dutch Continental Shelf, North Sea, Hollandse Kust (noord) Wind Farm Zone Survey 2017, 30 July to 01 September 2017 and 12 September to 03 November 2017, Fugro Report No.: GH216-R3, Project ID RVO.nl: WOZ2170055
Hamilton, 1985	EL Hamilton (1985) Sound velocity as a function of depth in marine sediments. J. Acoust. Soc. Am. 78 (4), 1348-1355
ISO 18405:2017	Underwater acoustics – Terminology
Kuperman & Ferla, 1985	Kuperman, W. A., & Ferla, M. C. (1985). A shallow water experiment to determine the source spectrum level of wind-generated noise. *The Journal of the Acoustical Society of America*, *77*(6), 2067-2073.
Merchant et al, 2015	Merchant, N.D., Fristrup, K.M., Johnson, M.P., Tyack, P.L., Witt, M.J., Blodel, P. and Parks, S.E. (2015) Measuring acoustic habitats, Methods in Ecology and Evolution, doi: 10.1111/2041-210X.12330
Merchant et al, 2018	Merchant, N., Farcas, A. and Powell, C. (2018) *Acoustic metric specification*, Report of the EU INTERREG Joint Monitoring Programme for Ambient Noise

	North Sea (Jomopans).
Ødegaard et al, 2019	Ødegaard, L., Pedersen, G., and Johnson, E., (2019). Underwater noise from wind at the high north LoVe ocean observatory. UACE2019 - Conference Proceedings. 1-8.
Putland et al, 2021	Putland, R.L., Farcas, A., Merchant, N. D. (2021) *Uncertainty assessment between measurements and model predictions: Final report*. Report of the EU INTERREG Joint Monitoring Programme for Ambient Noise North Sea (Jomopans)
Rees, 2003	Rees, T. (2003) *"C-Squares", a New Spatial Indexing System and its Applicability to the Description of Oceanographic Datasets*, Oceanography 16(1), pp.11-19
Sertlek et al, 2016	H.Ö. Sertlek, B. Binnerts and M.A. Ainslie (2016) The effect of sound speed profile on shallow water shipping sound maps, J. Acoust. Soc. Am. 140 (1), EL84-88
Siderius & Porter, 2008	Siderius, M., & Porter, M. B. (2008). Modeling broadband ocean acoustic transmissions with time-varying sea surfaces. J. Acoust. Soc. Am. 124(1), pp 137–150
Thorp, 1967	Thorp, W.H. (1967) *Analytic Description of the Low-Frequency Attenuation Coefficient.* Journal of the Acoustical Society of America, Vol. 42, p. 270
van Moll et al, 2009	Camiel A. M. van Moll, Michael A. Ainslie, and Robbert van Vossen; A Simple and Accurate Formula for the Absorption of Sound in Seawater; (2009) IEEE Journal of Oceanic Engineering, Vol. 34, NO. 4, pp.610-616
Wang & Robinson, 2020	JOMOPANS terminology standard, V2
Weston & Ching, 1998	David E. Weston and PamelaA. Ching (1998) Wind effects in shallow-water acoustic transmission. J. Acoust. Soc. Am. 86(4), 1530-1545
Zhou et al 2009	Ji-Xun Zhou, Xue-Zhen Zhang & D. P. Knobles (2009) Low-frequency geoacoustic model for the effective properties of sandy seabottoms, J. Acoust. Soc. Am. 125(5), 2847–2866

Annex A AIS data and model visualisations

In this the subsequent section of this appendix, the following figures are found for all 2018 sites (excluding the love station for which a separate analysis has been carried out as part of the WP6 report [Farcas et al, 2020]).

- The set of figure shows per location and per vessel class, maps of the vessel density in the month of the measurements in 2018. All figures have the same dynamic range and show a normalised logarithmic 10*log10(sum number of ships in grid cell). The black dot indicates the hydrophone location.
- The second set of figures shows (per location and per vessel type):
  - The number of vessels in the AIS recording for the 2018 measurement period
  - Percentiles of the length distribution (over vessels)
  - Percentiles of the speed distribution (over vessels and time)
  - Percentiles of the distance to the measurement station (over vessels and time)
  - Percentiles of the RANDI3.1c prediction of the broadband source level (over vessels and time)
- A visualisation of the modelled noise for the first and second iteration

Annex A.1 Sweden – Vinga

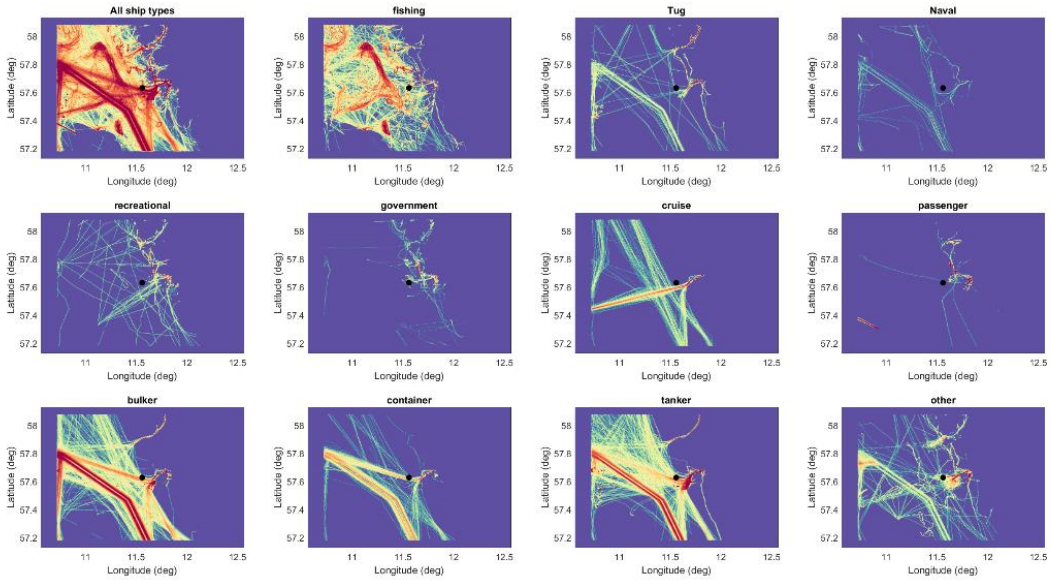

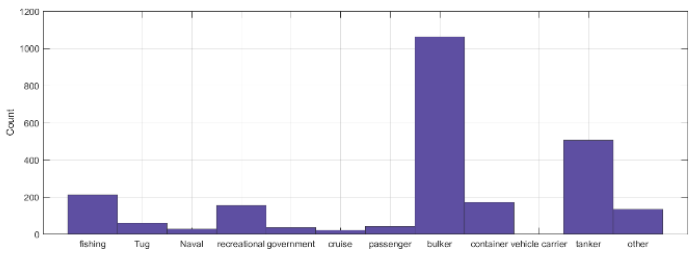

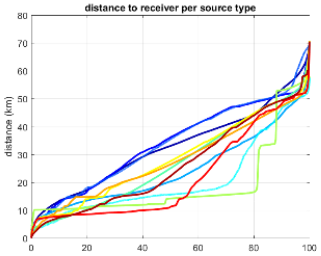

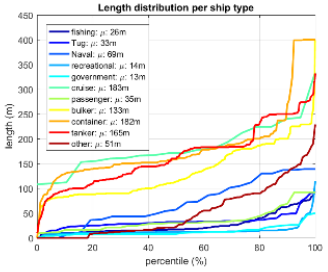

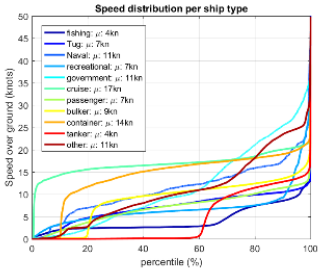

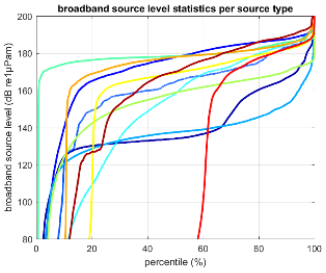

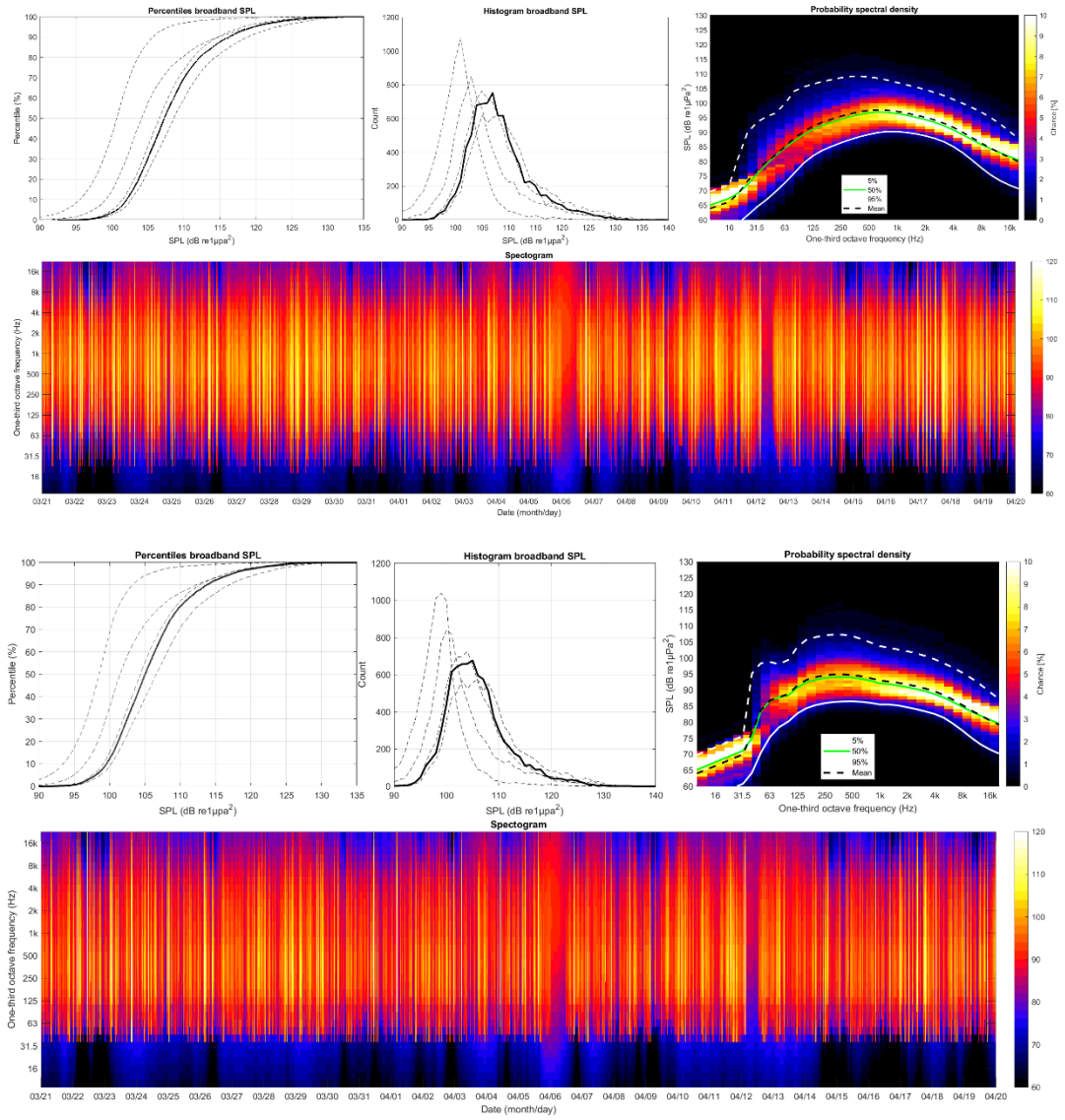

Figure 11 First iteration (top) and second iteration (bottom) calculated SPL at 1 m above the sea floor for the period in 2018 over which underwater sound was recorded at the Swedish Vinga station.

Annex A.2 Denmark – Anholt

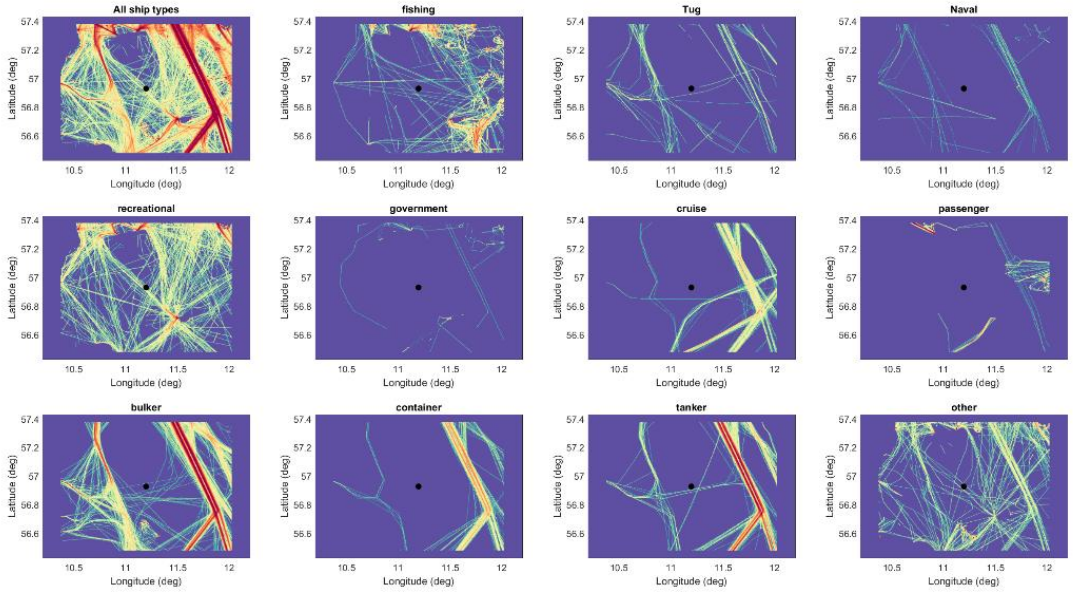

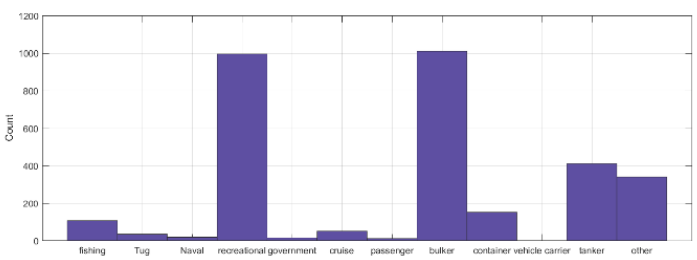

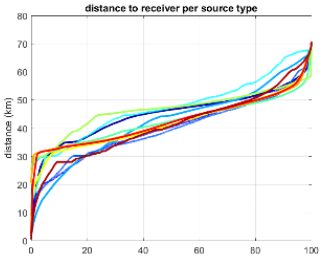

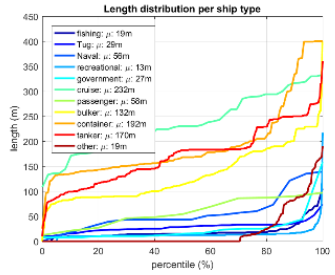

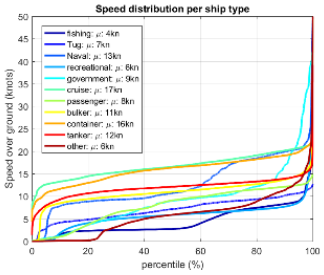

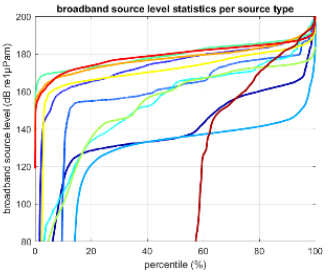

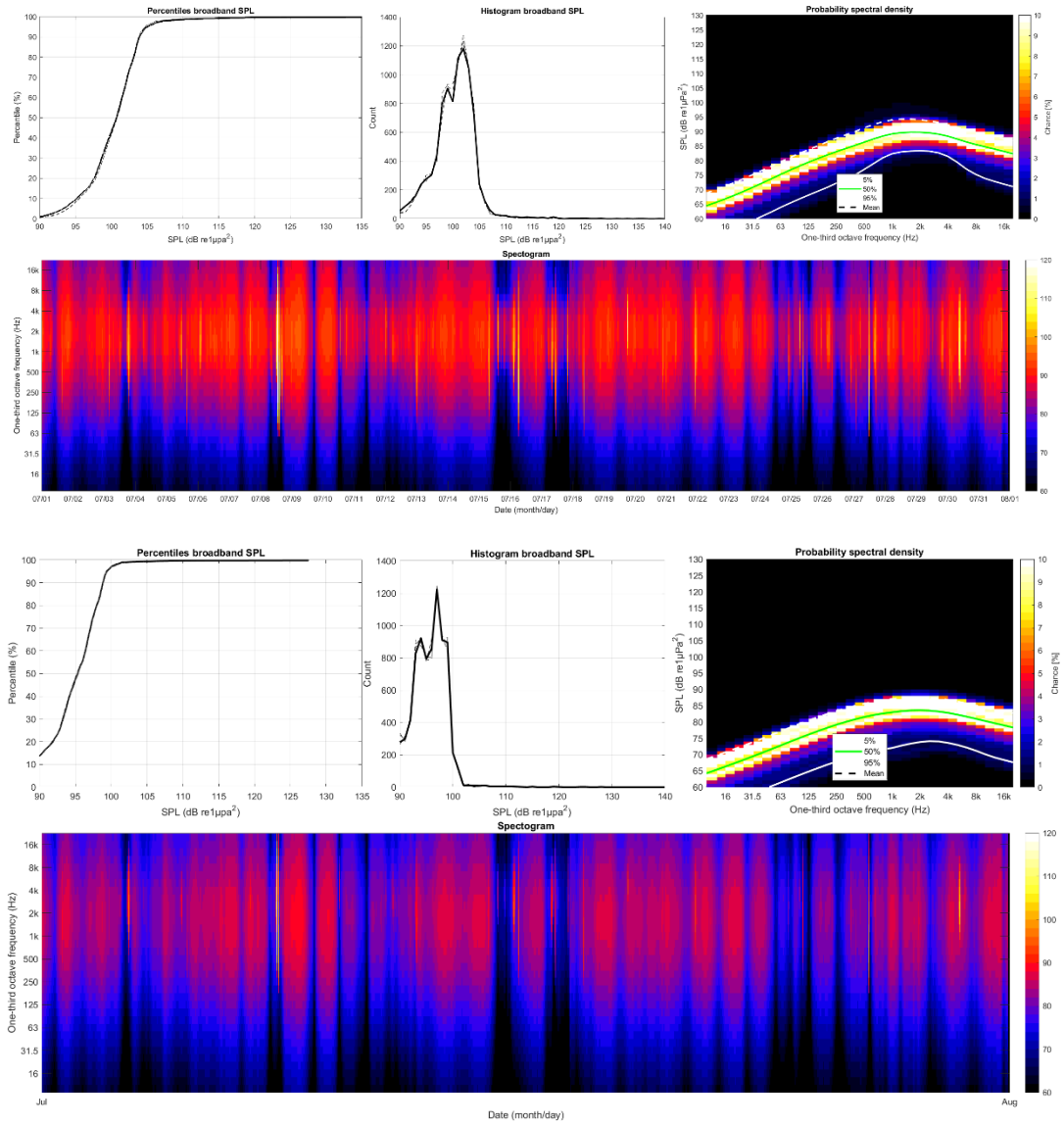

Figure 12 First iteration (top) and second iteration (bottom) calculated SPL at 1 m above the sea floor for the period in 2018 over which underwater sound was recorded at the Danish Anholt station.

Annex A.3 Netherlands – Texel

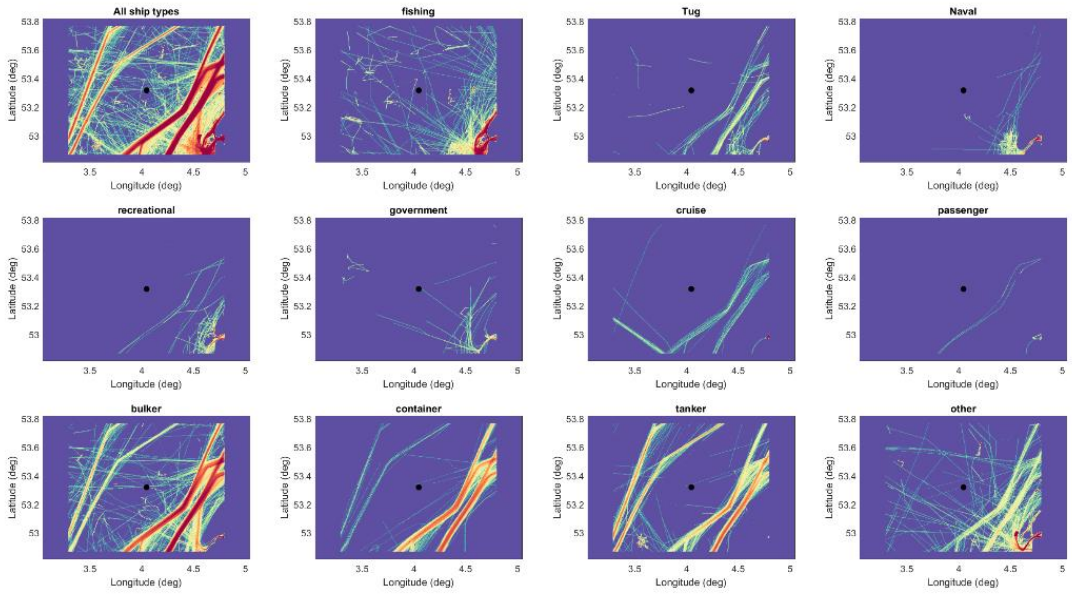

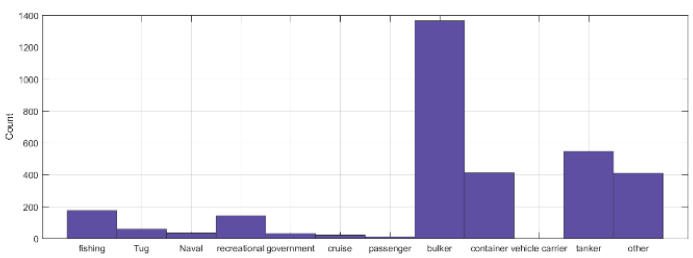

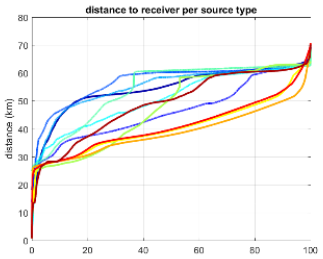

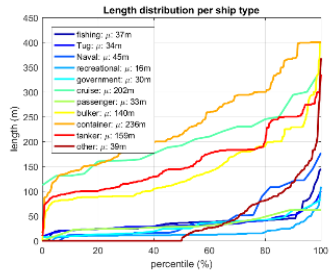

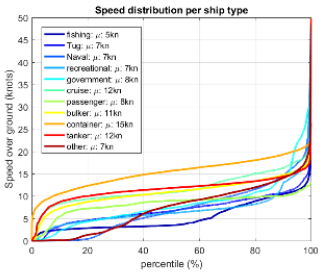

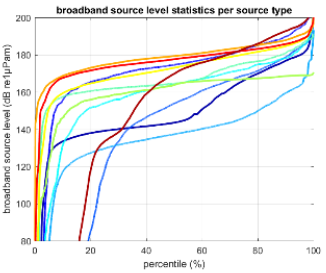

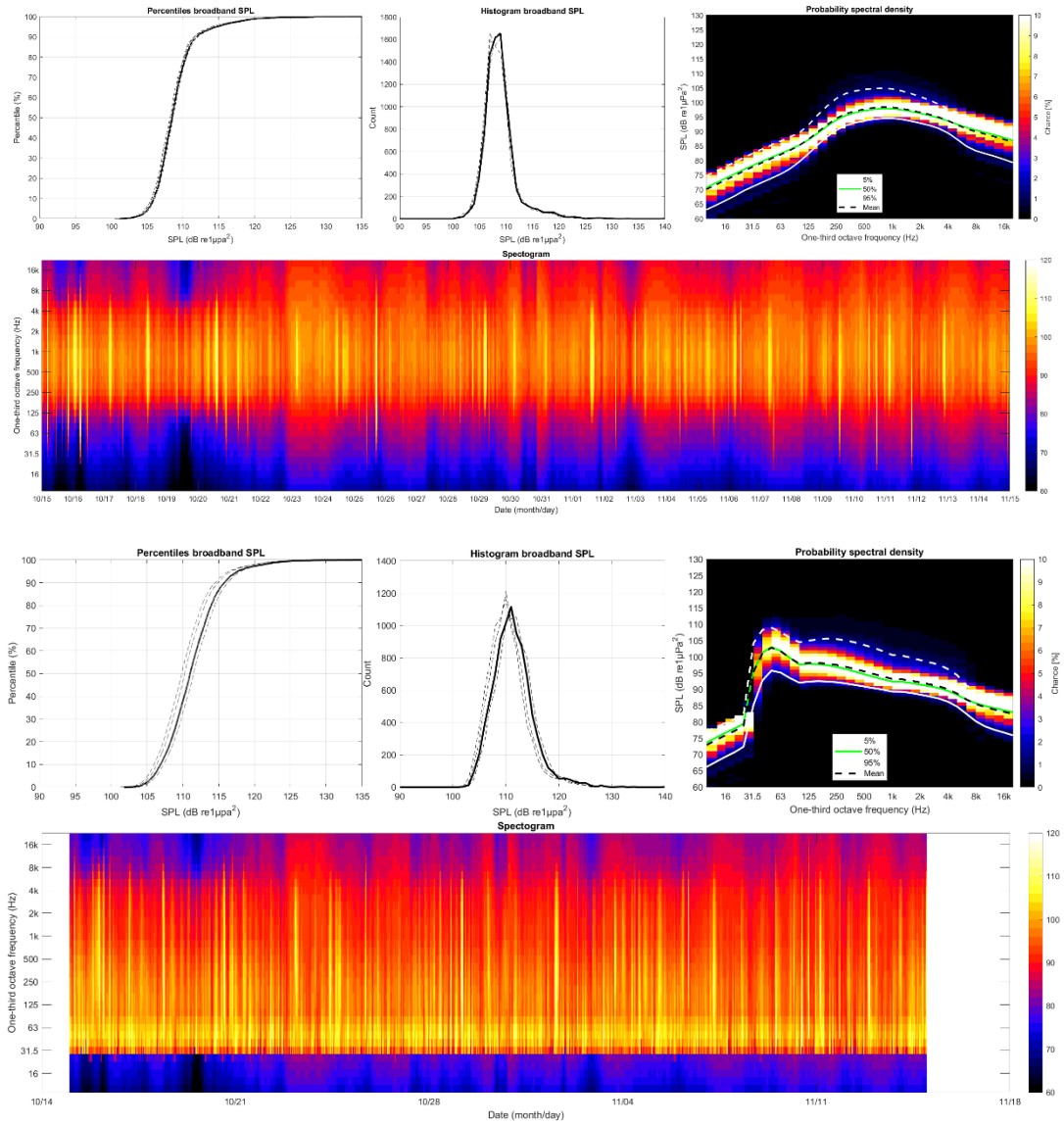

Figure 13 First iteration (top) and second iteration (bottom) calculated SPL at 1 m above the sea floor for the period in 2018 over which underwater sound was recorded at the Dutch Texel station.

Annex A.4 England – Dowsing

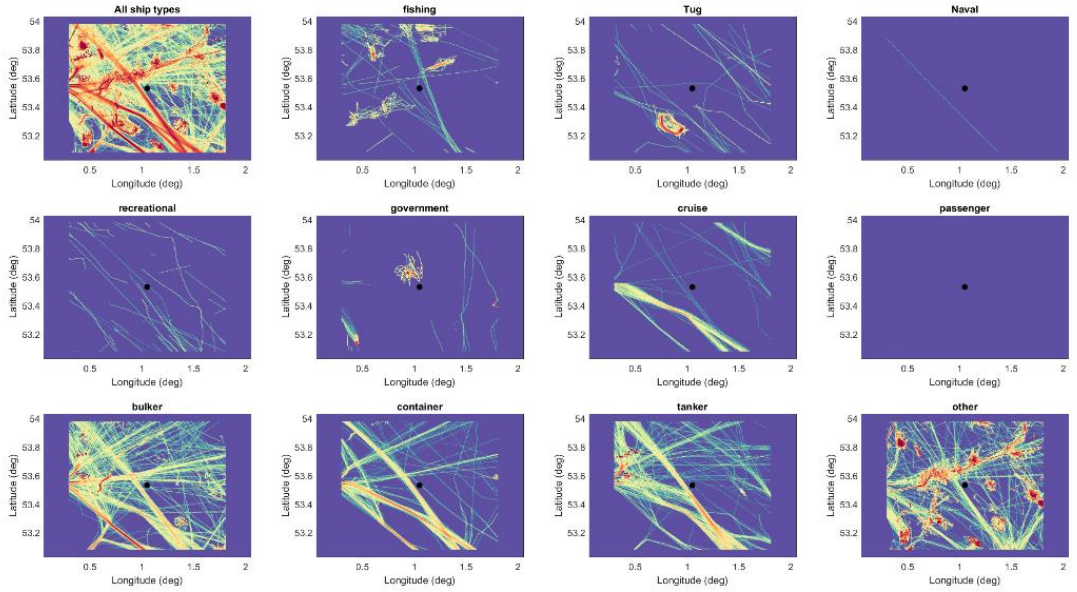

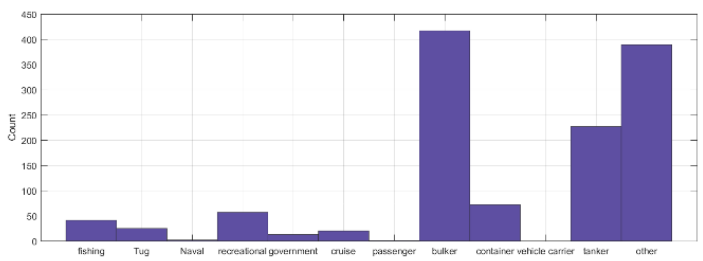

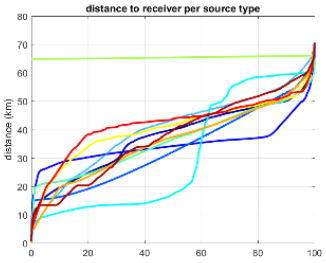

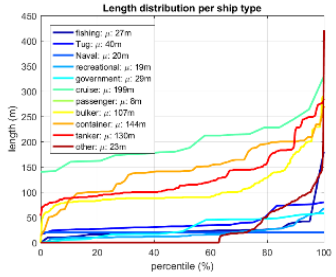

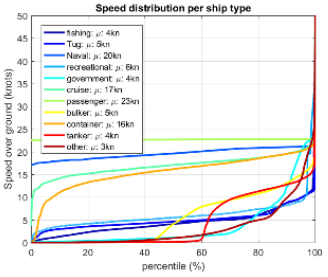

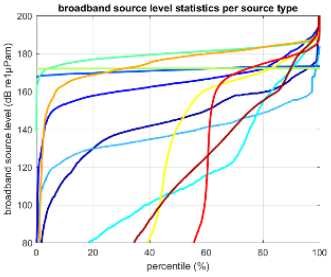

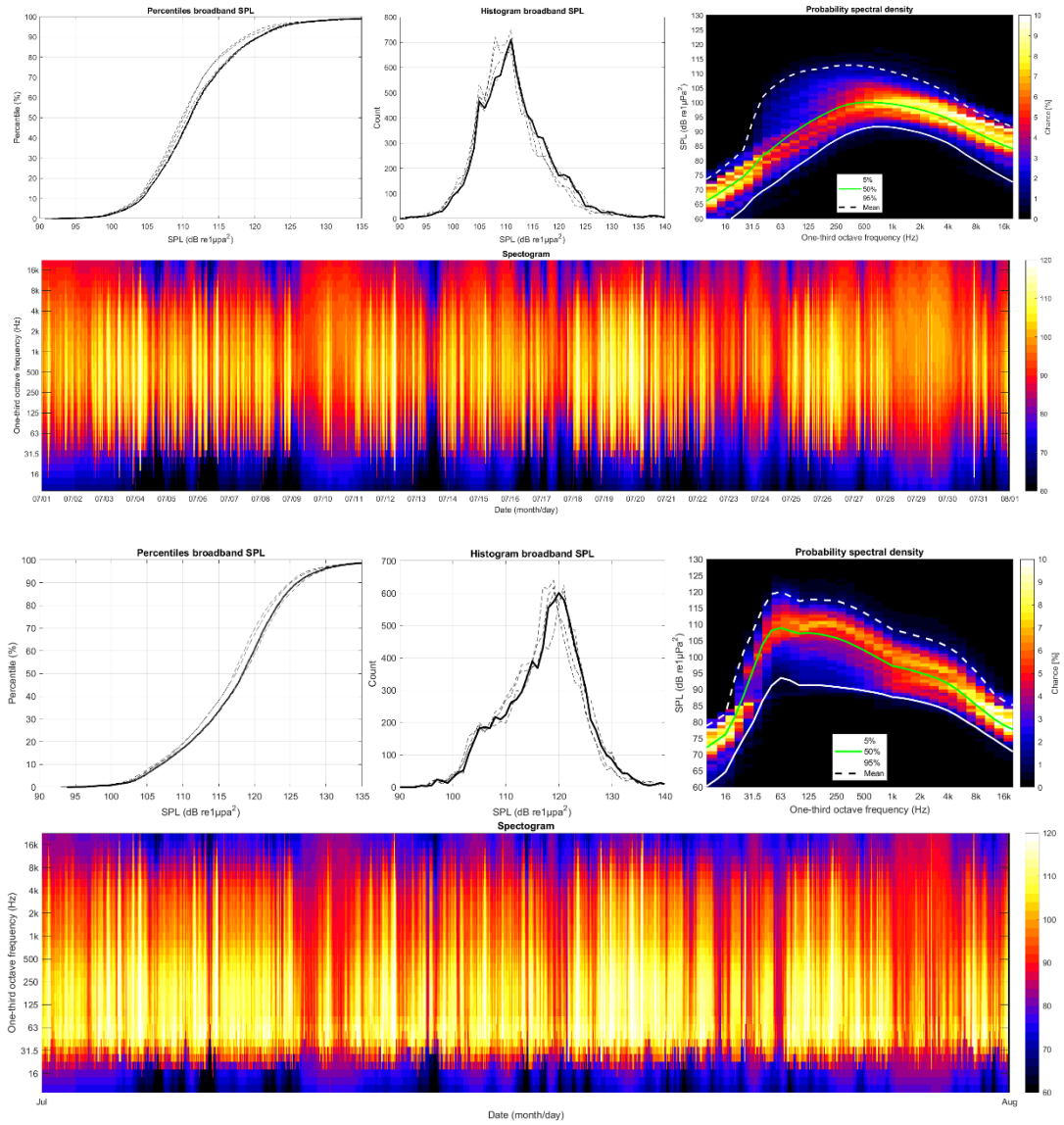

Figure 14 First iteration (top) and second iteration (bottom) calculated SPL at 1 m above the sea floor for the period in 2018 over which underwater sound was recorded at the English Dowsing station.

Annex A.5 Scotland – Helmsdale

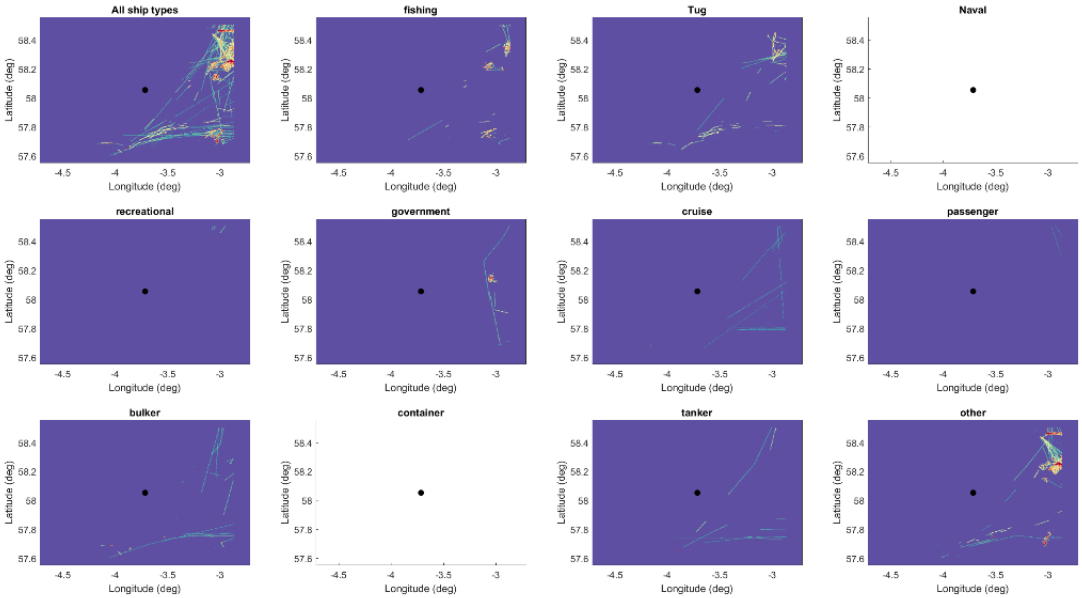

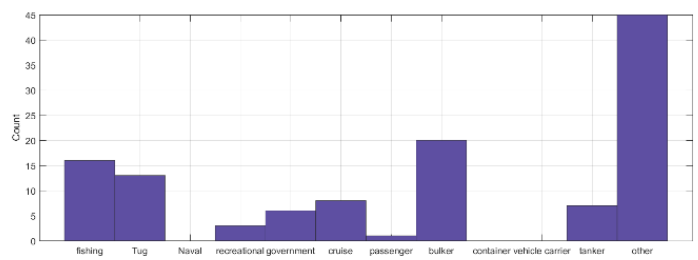

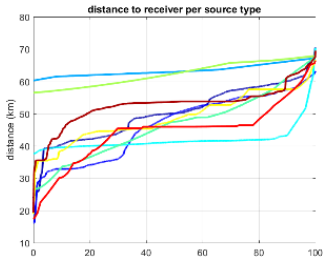

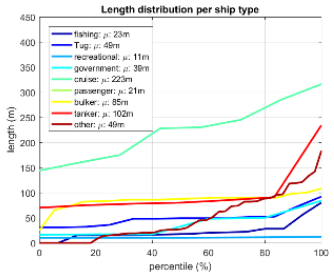

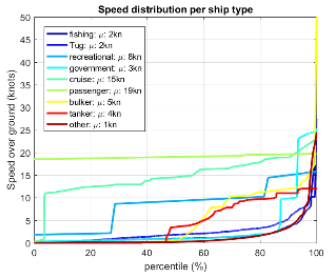

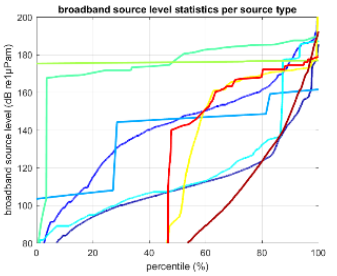

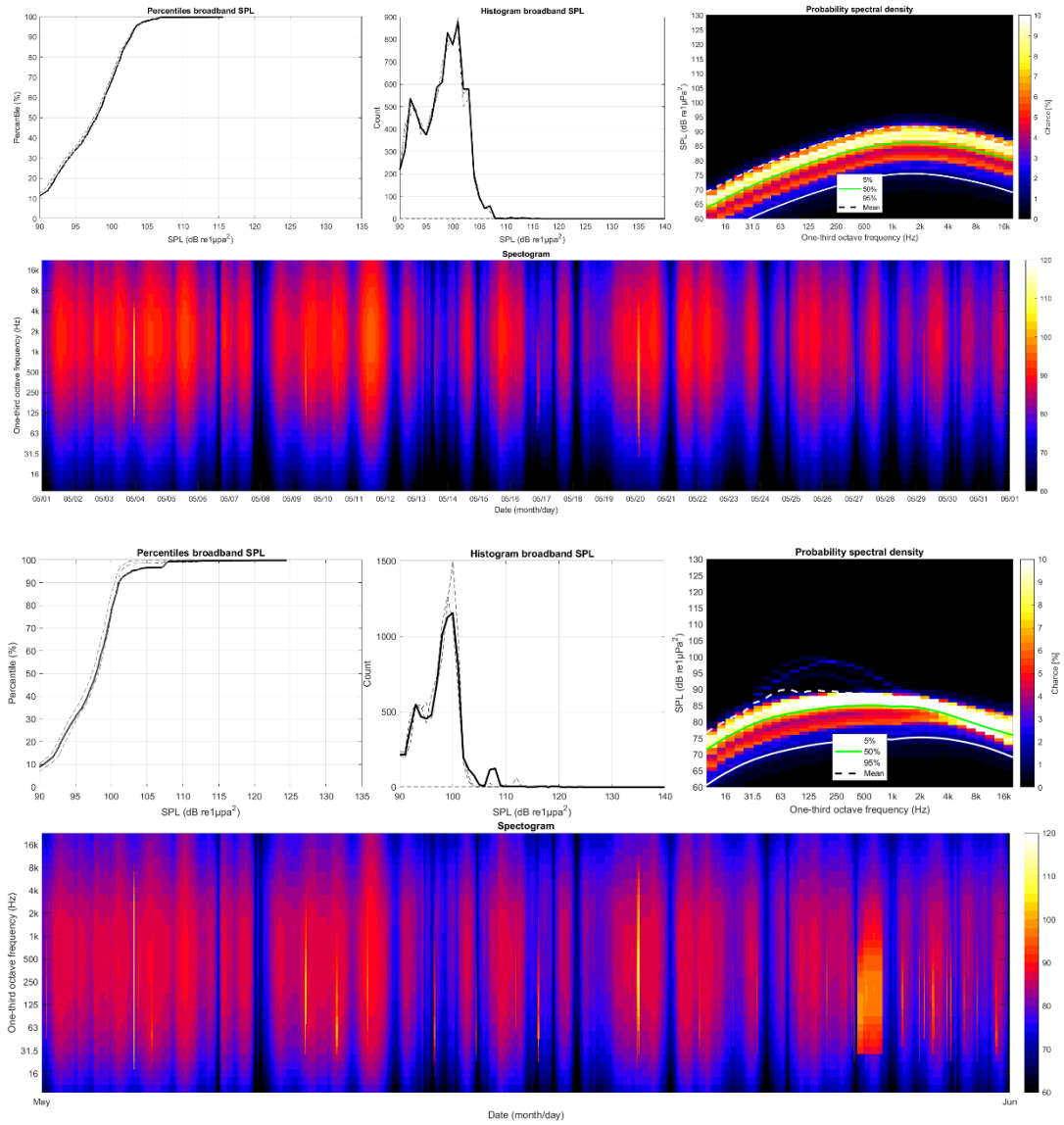

Figure 15 First iteration (top) and second iteration (bottom) calculated SPL at 1 m above the sea floor for the period in 2018 over which underwater sound was recorded at the Scottish Helmsdale station.

Annex A.6 Scotland – Moray Firth

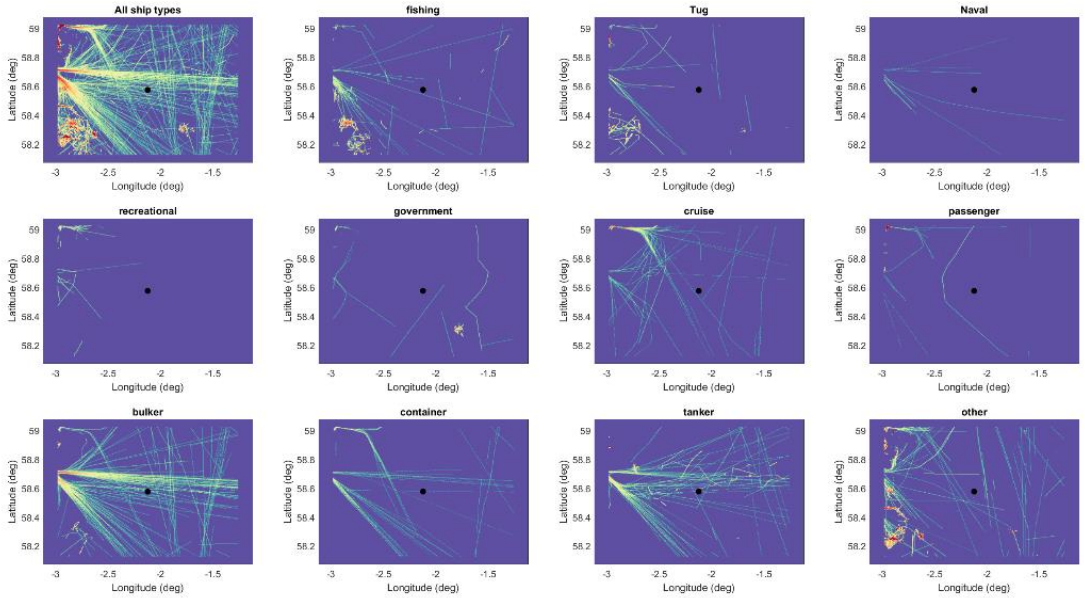

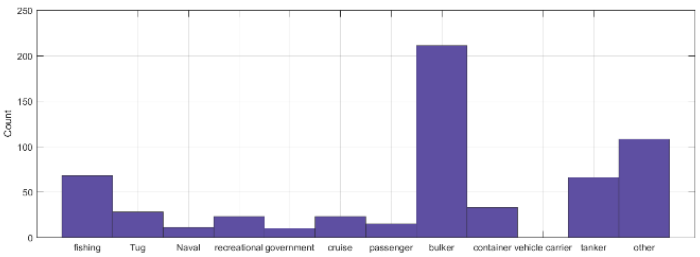

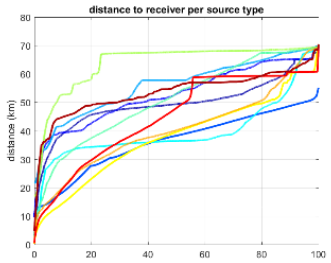

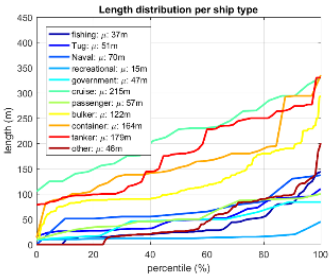

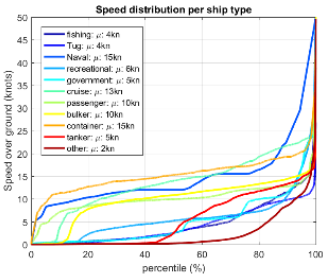

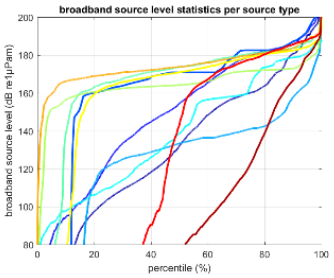

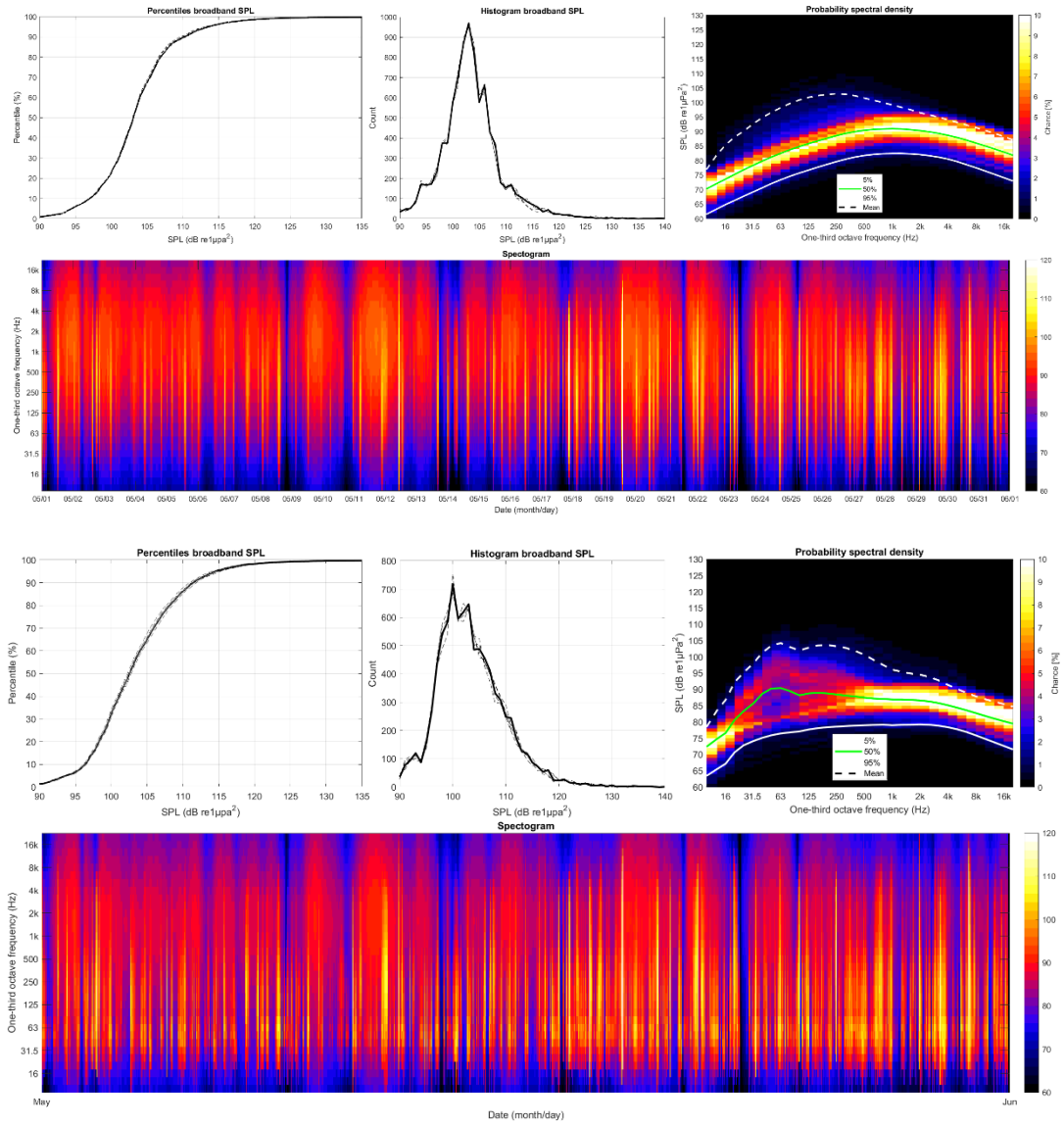

Figure 16 First iteration (top) and second iteration (bottom) calculated SPL at 1 m above the sea floor for the period in 2018 over which underwater sound was recorded at the Scottish Moray Firth station.

Annex B Comparison of WP4 partner modelling results

Shipping swedenVinga

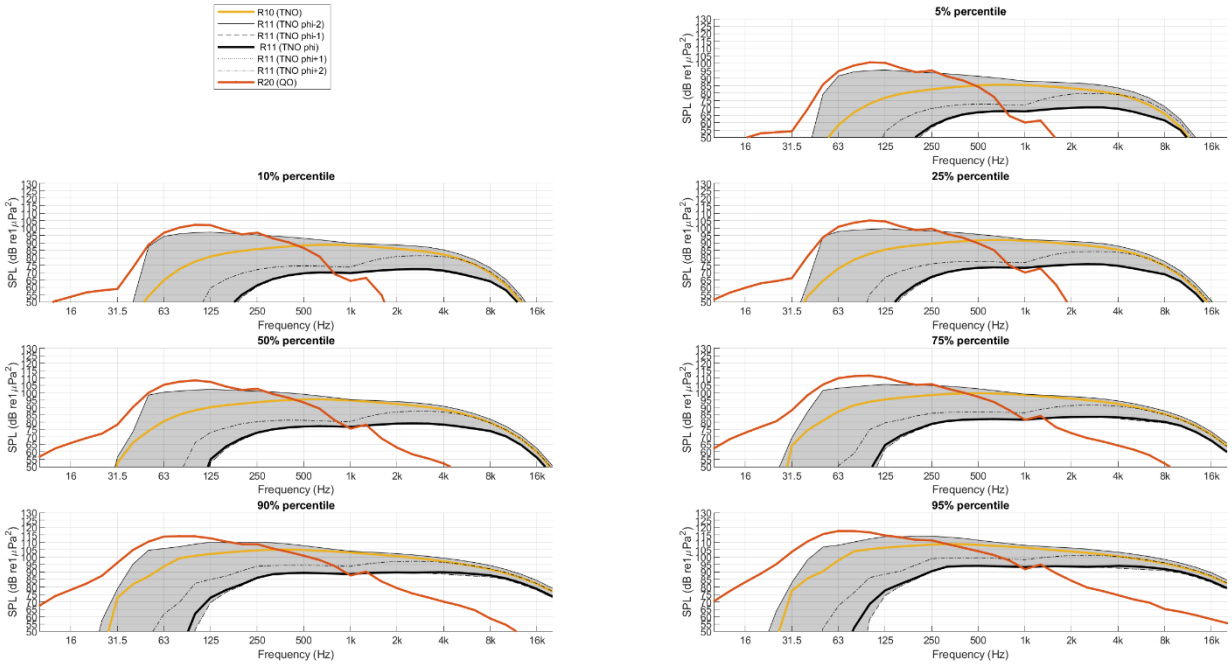

Wind swedenVinga

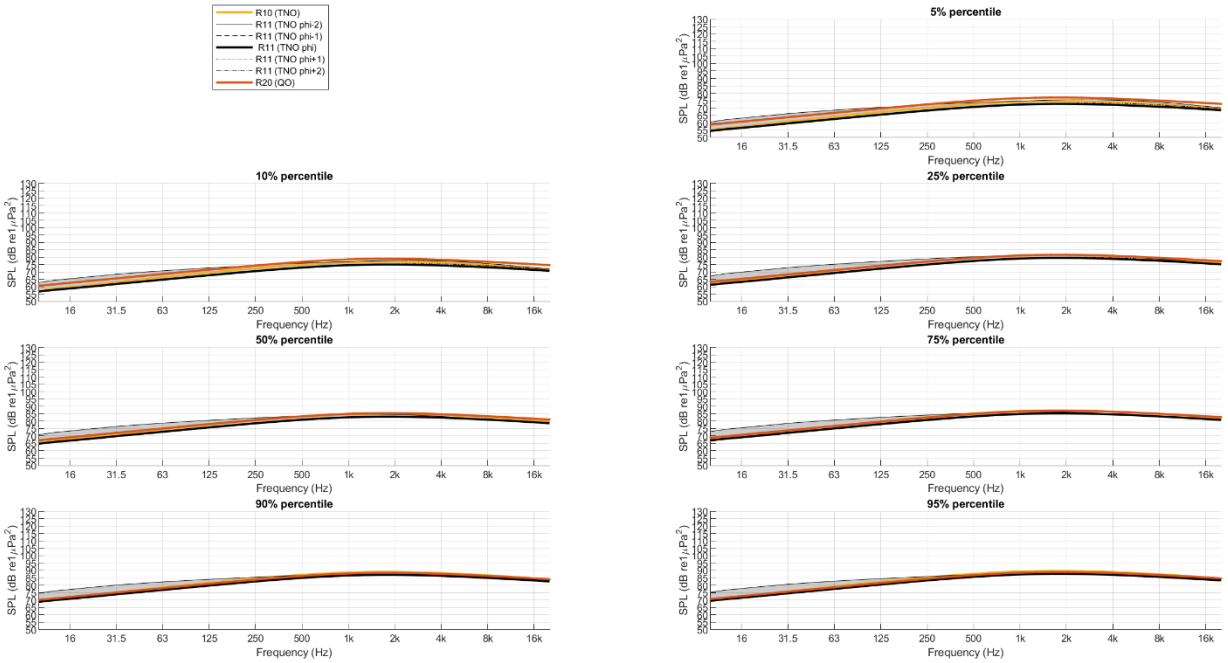

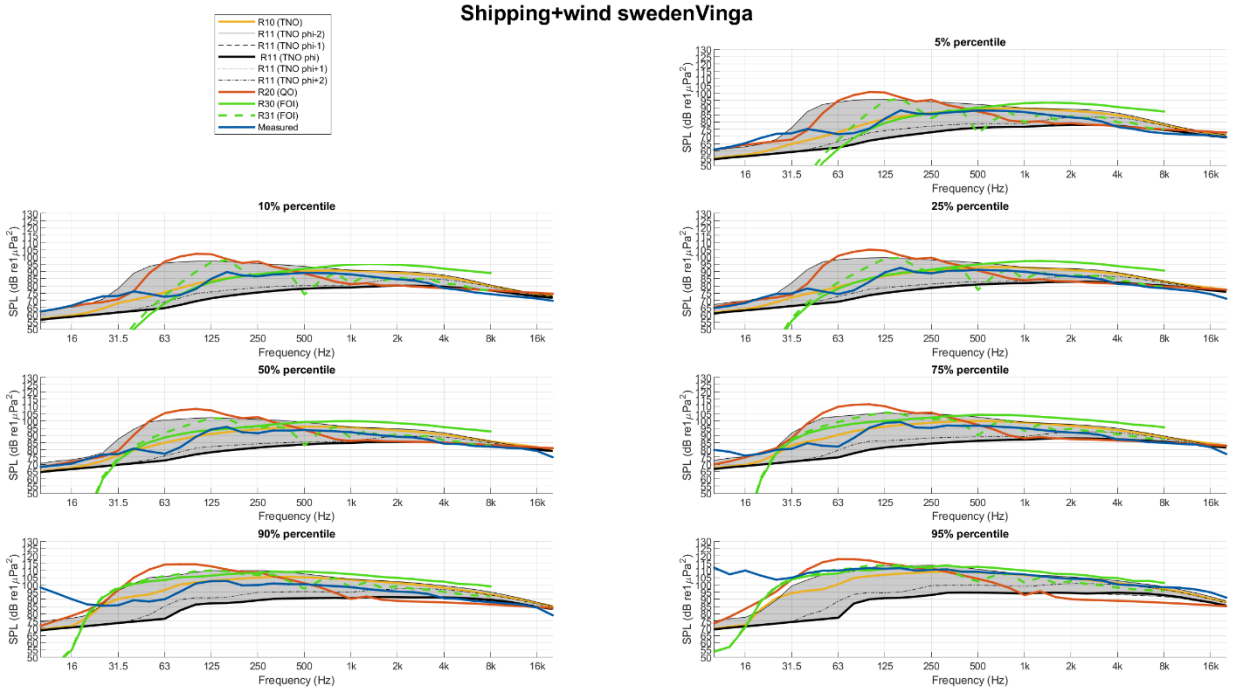

Figure 17: model-data comparison for 2018 site #1 (Vinga, Sweden). One-third octave (base-10) band spectra of the SPL percentiles at the measurement location. TNO predictions (shaded area) are for a range of sediment types.

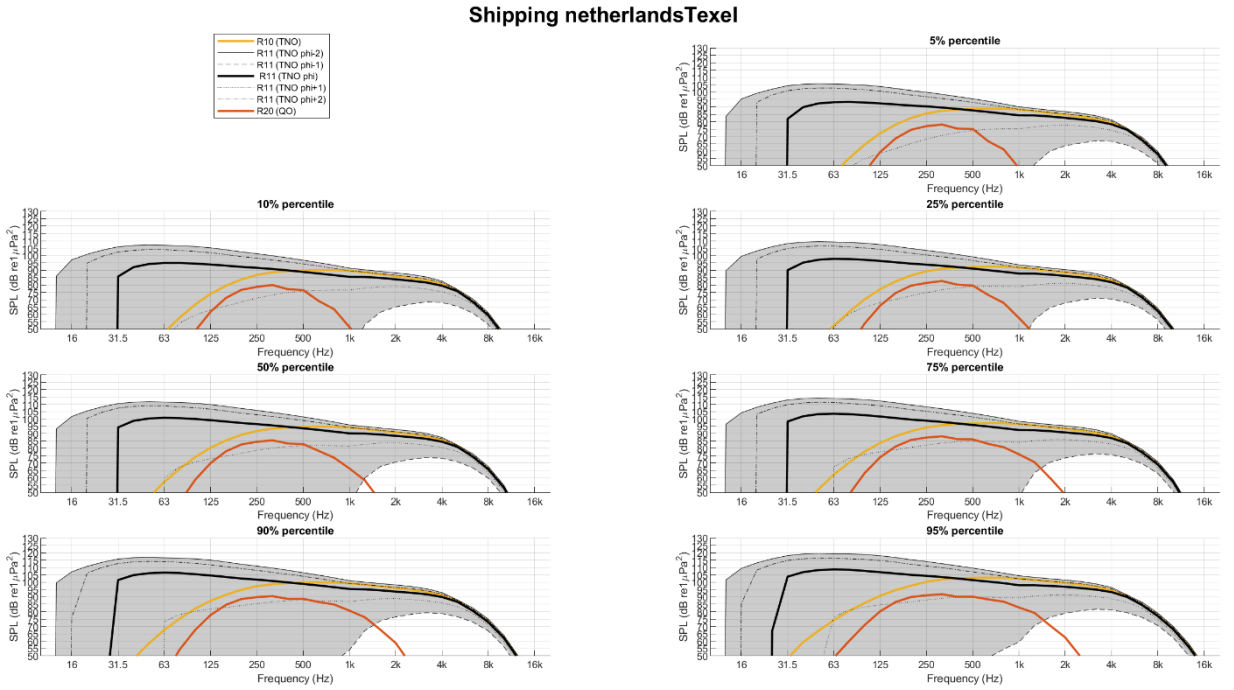

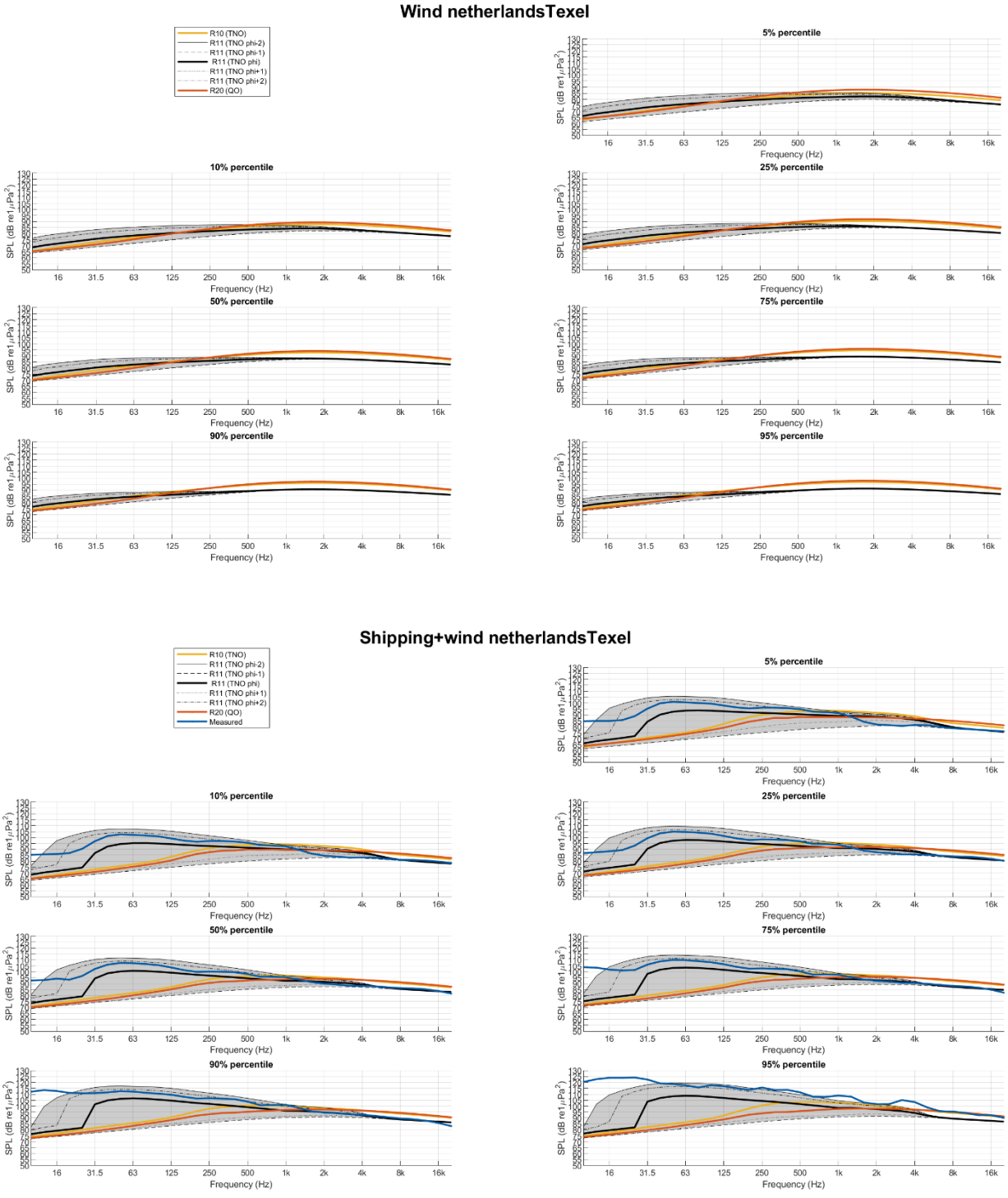

Figure 18: model-data comparison for 2018 site #4 (Texel, Netherlands). One-third octave (base-10) band spectra of the SPL percentiles at the measurement location. TNO predictions (shaded area) are for a range of sediment types.

Shipping englandDowsing

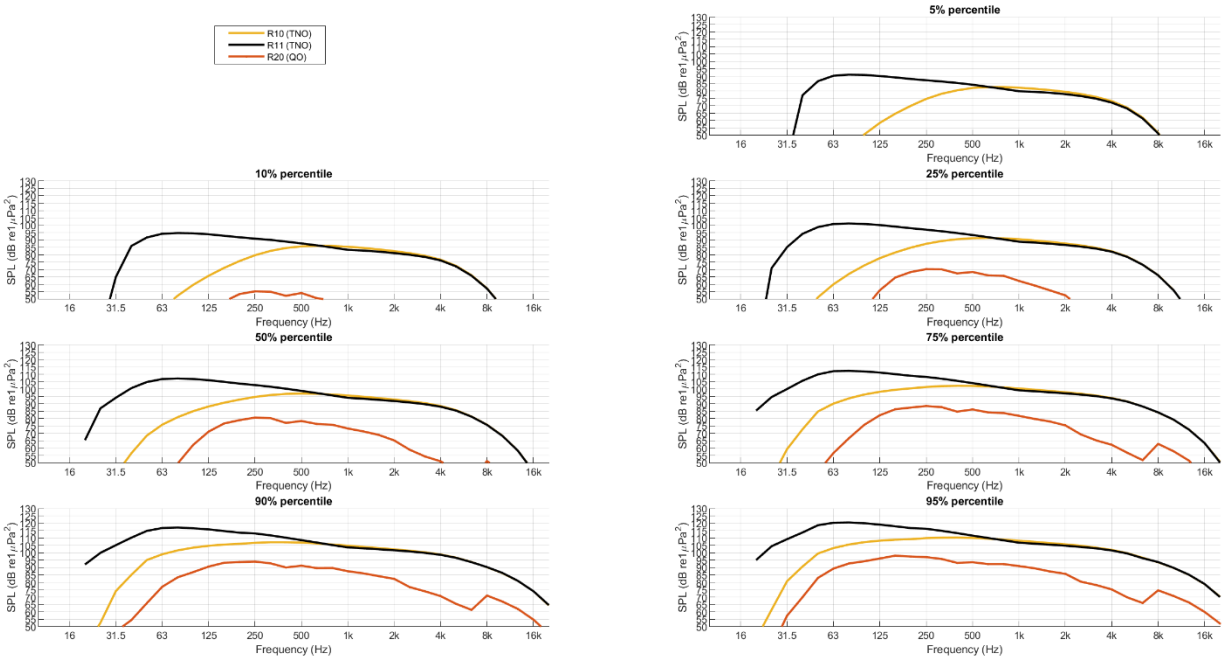

Wind englandDowsing

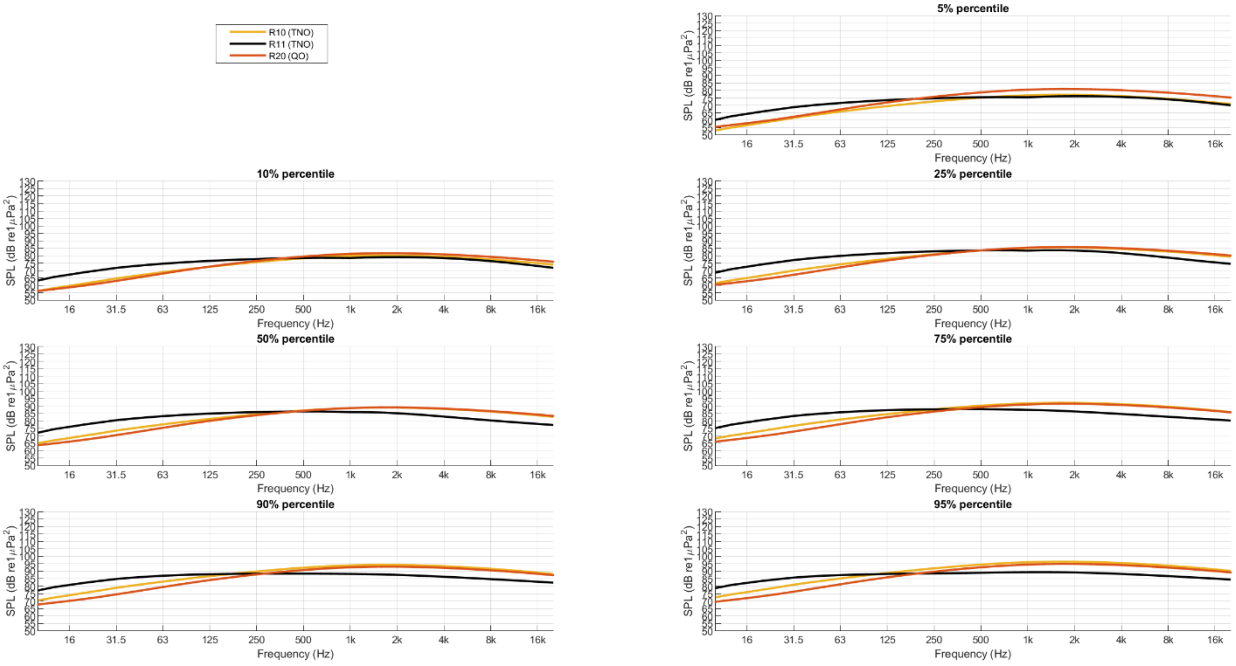

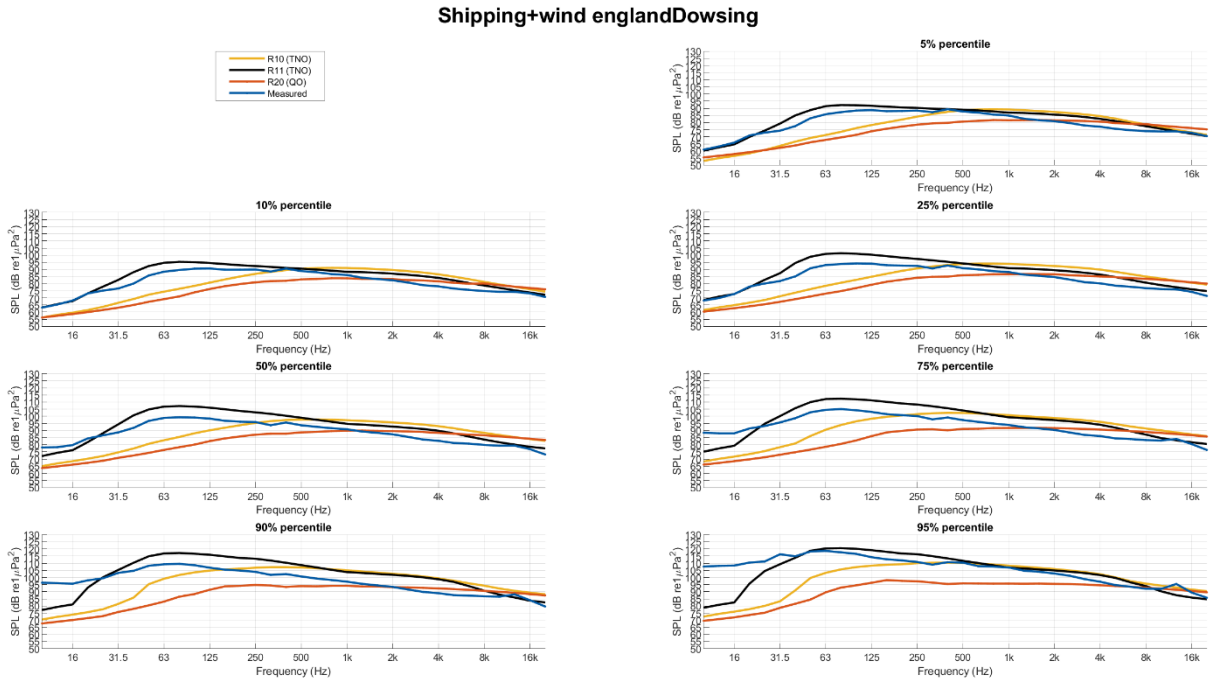

Figure 19: model-data comparison for 2018 site #5 (Dowsing, England). One-third octave (base-10) band spectra of the SPL percentiles at the measurement location.

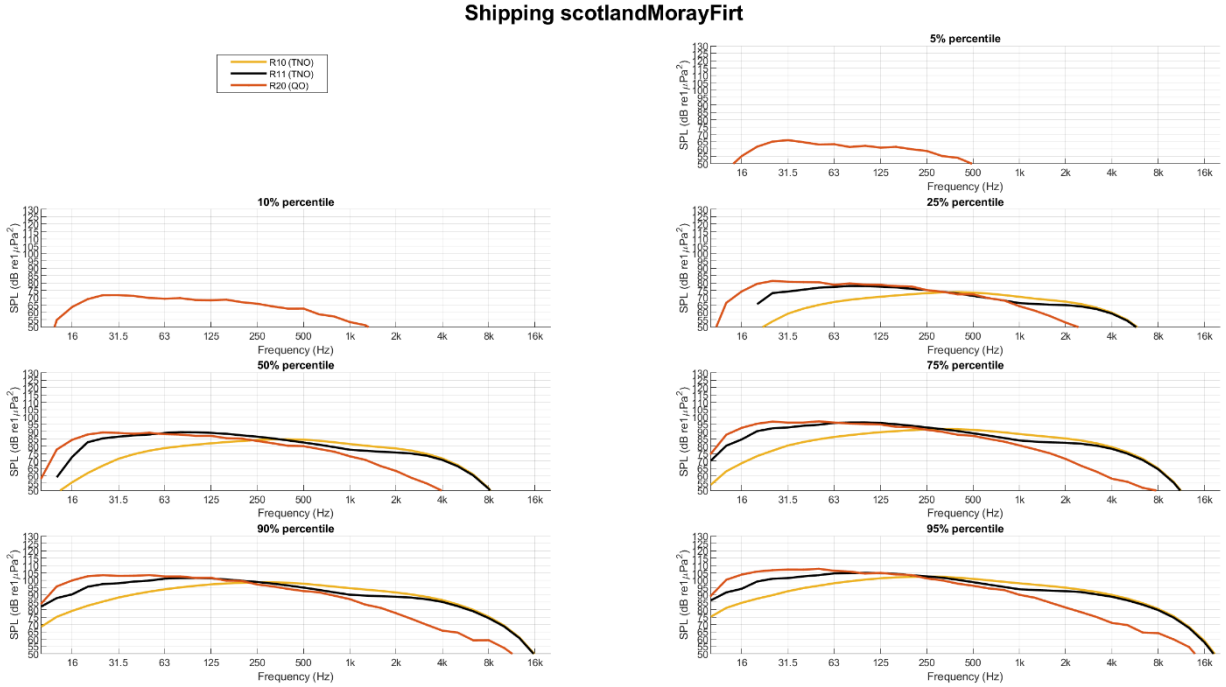

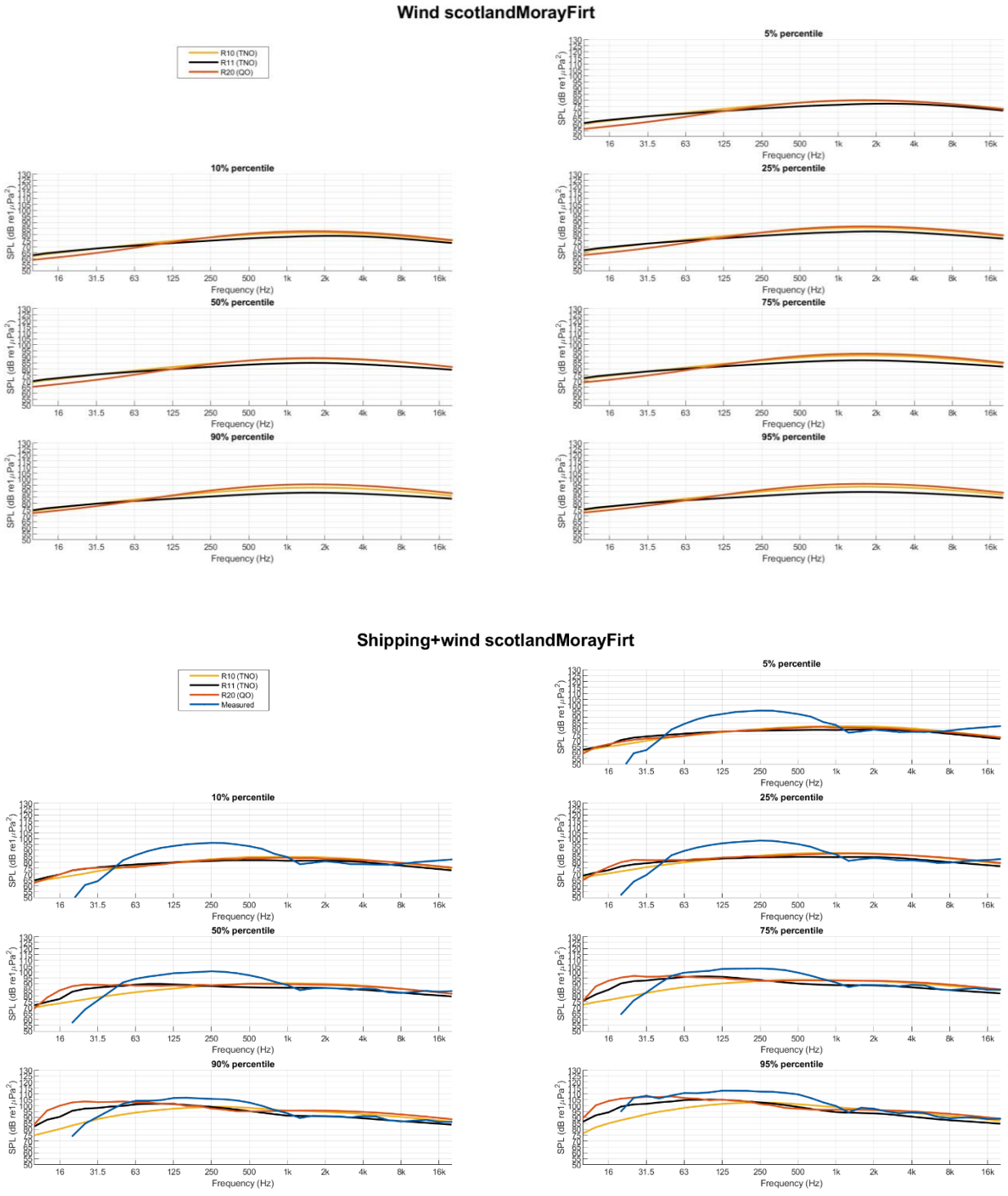

Figure 20: model-data comparison for 2018 site #7 (Moray Firth, Scotland). One-third octave (base-10) band spectra of the SPL percentiles at the measurement location.

Shipping denmarkAnholt

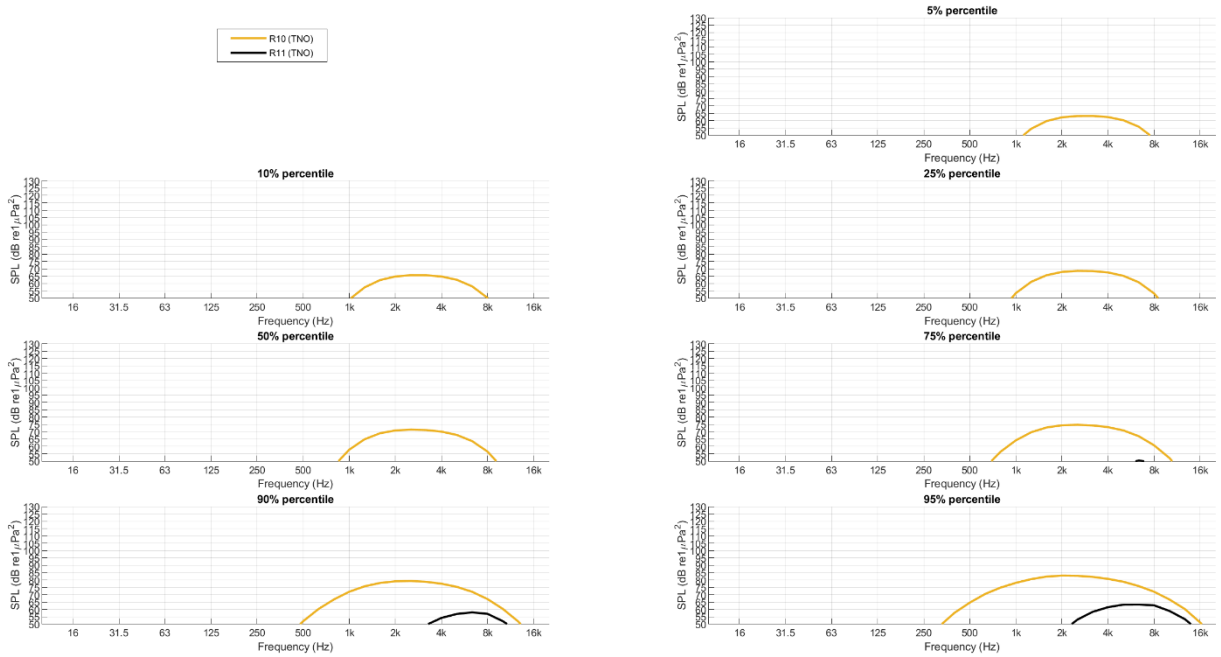

Wind denmarkAnholt

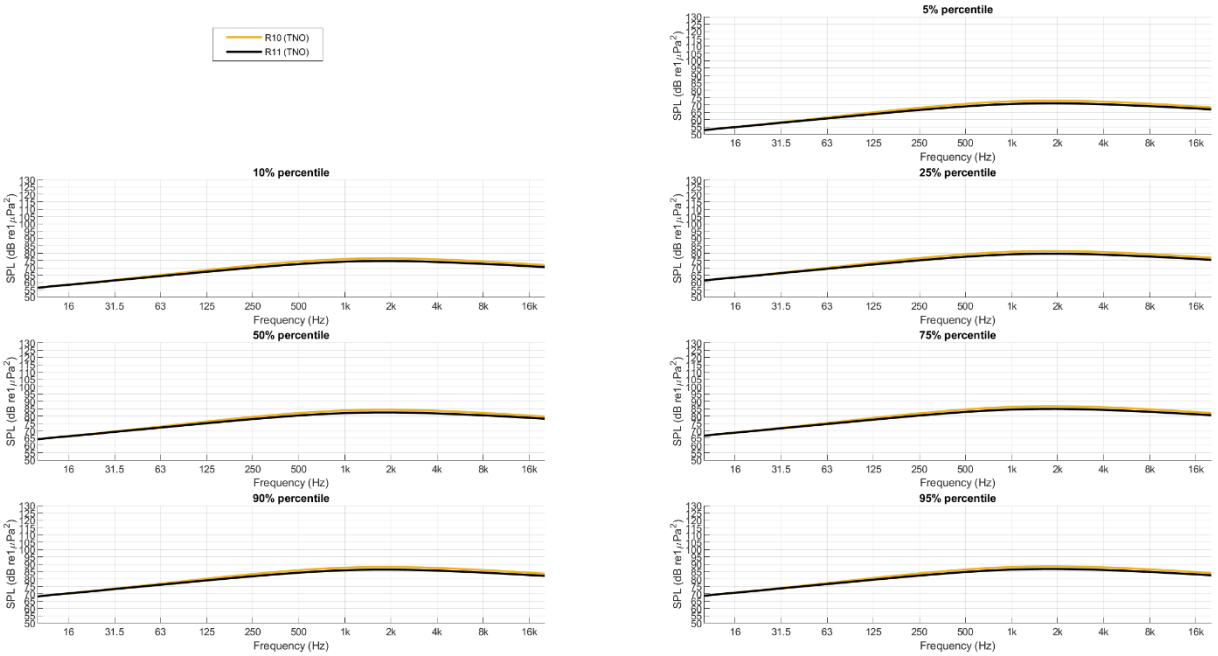

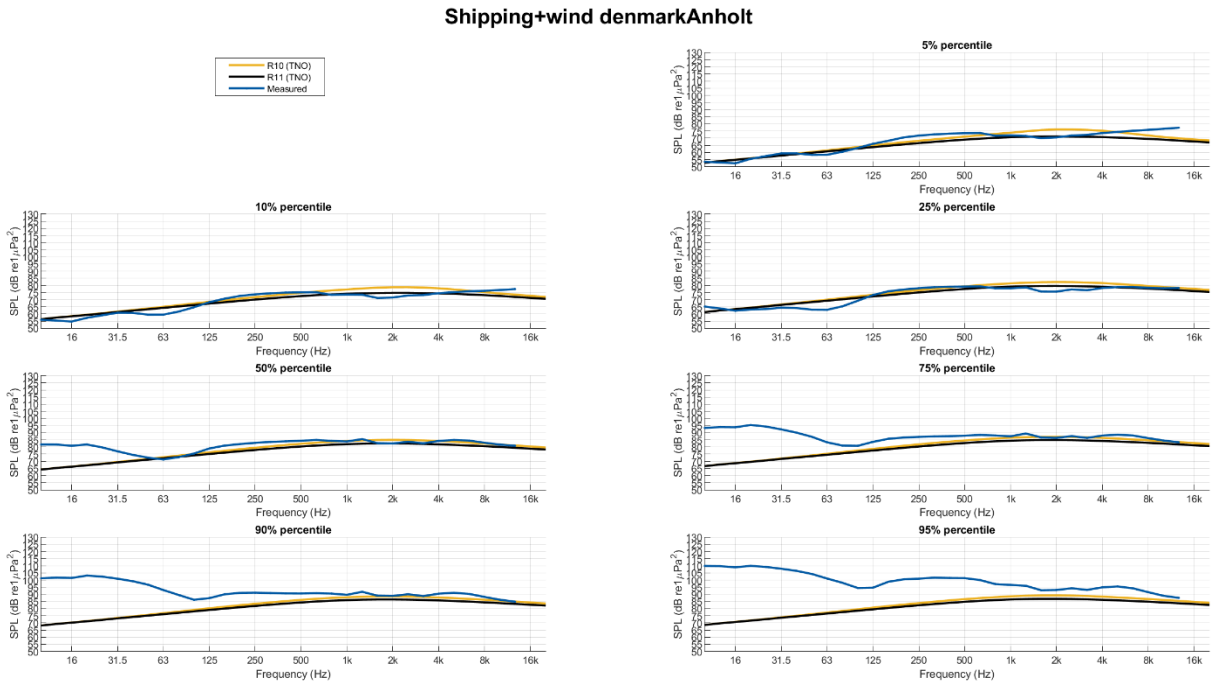

Figure 21: model-data comparison for 2018 site #2 (Anholt, Denmark). One-third octave (base-10) band spectra of the SPL percentiles at the measurement location.

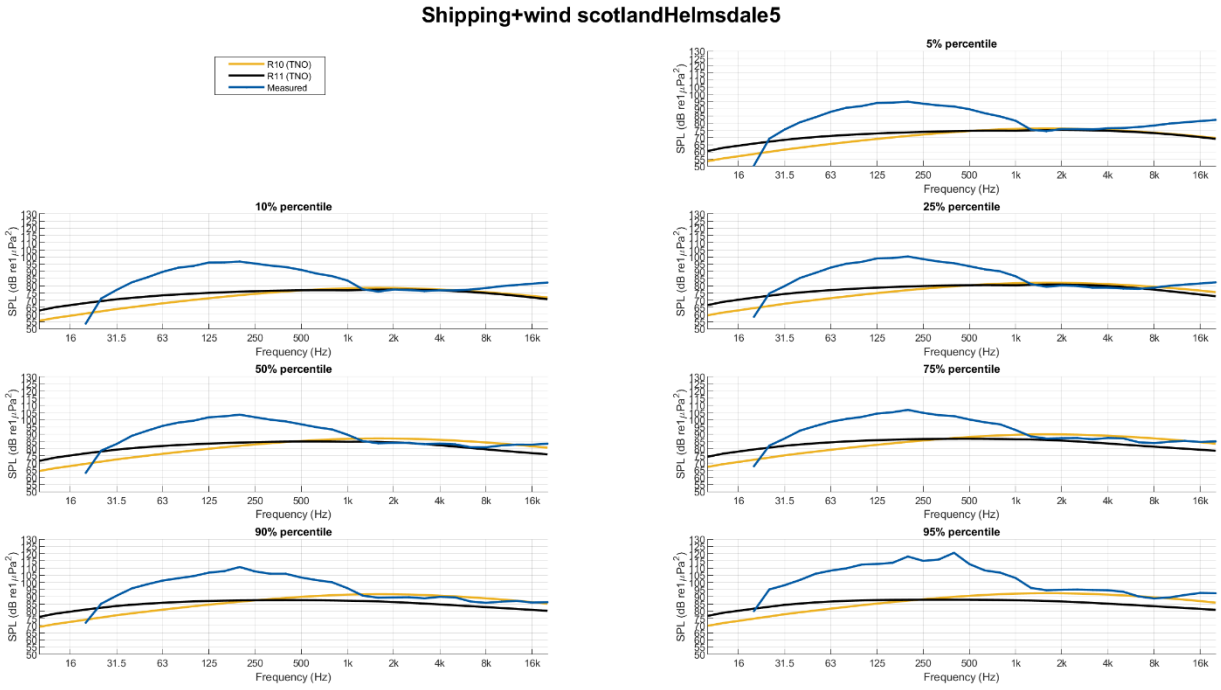

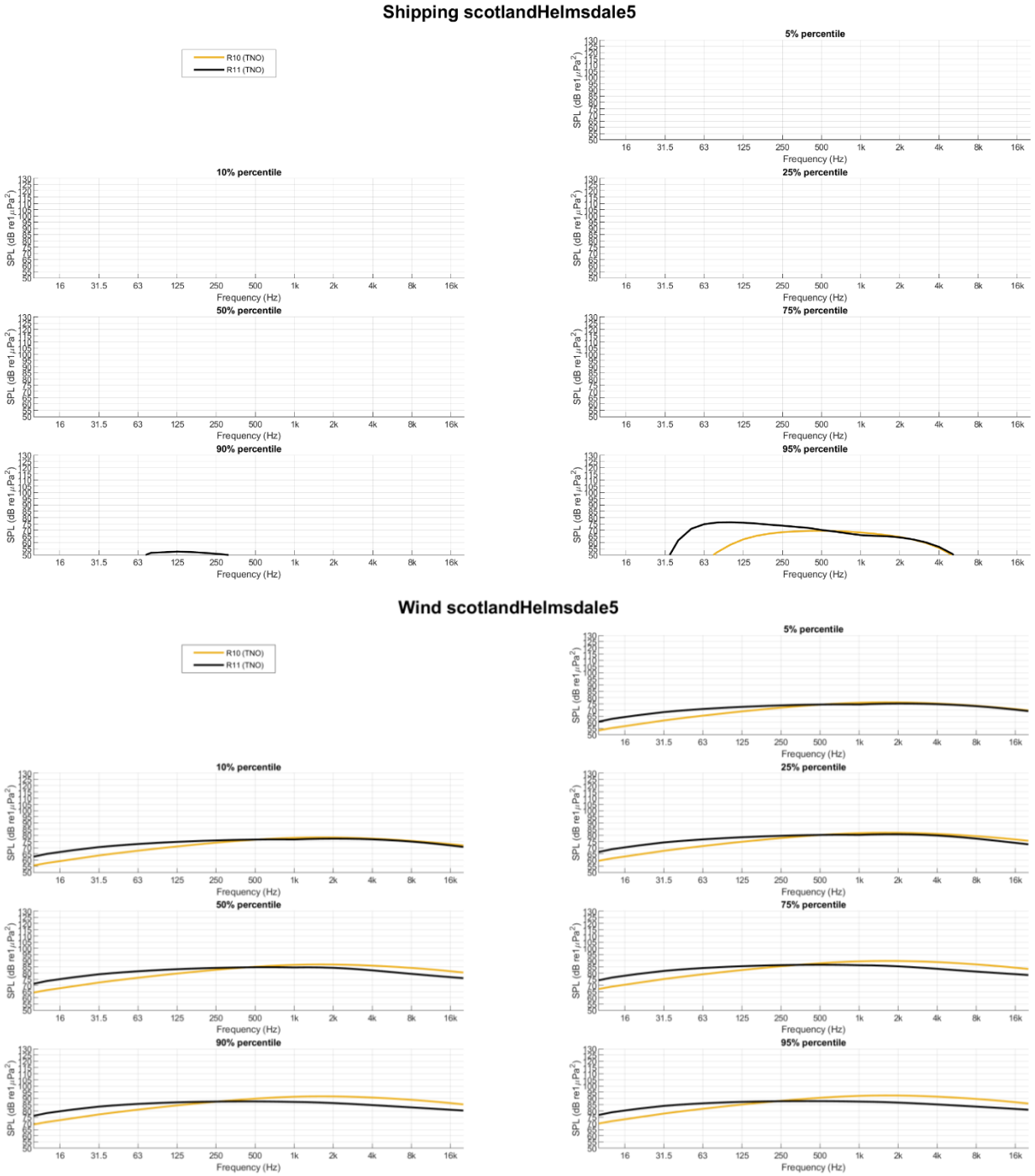

Figure 22: model-data comparison for 2018 site #6 (Helmsdale, Scotland). One-third octave (base-10) band spectra of the SPL percentiles at the measurement location.

Annex C Wind noise modelling results

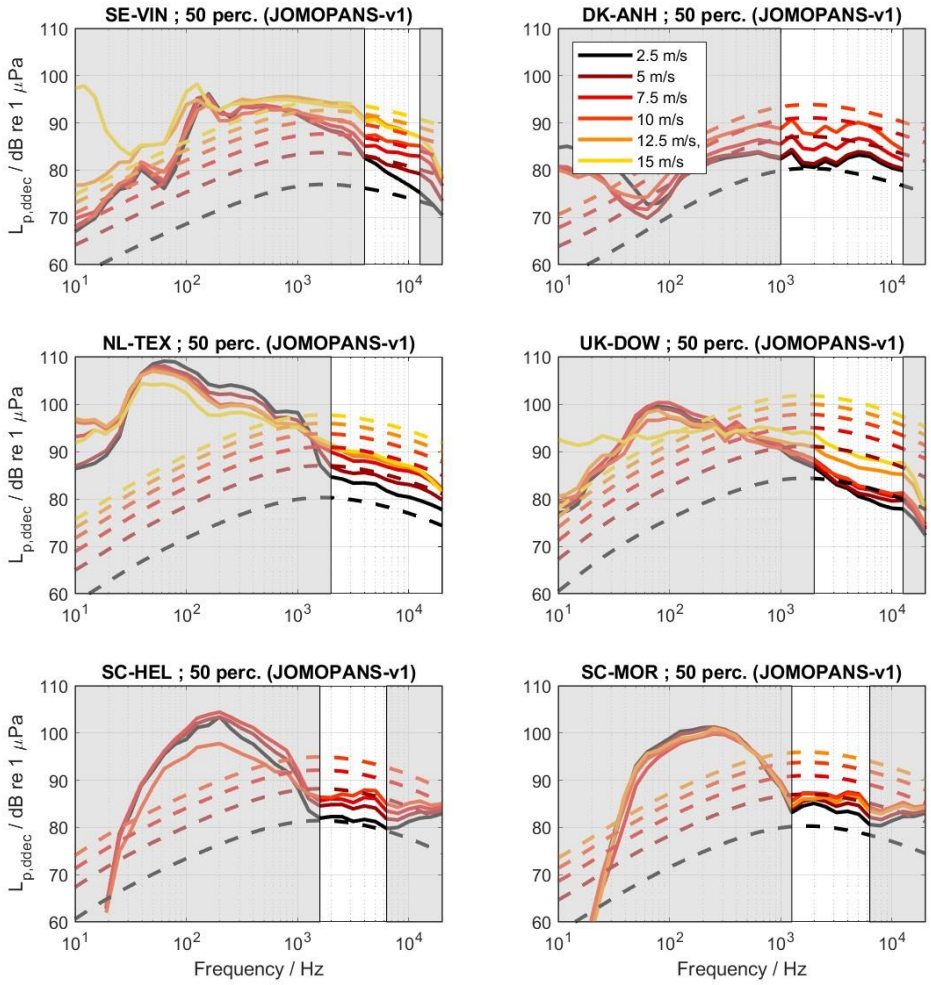

Figure 23 Comparison of JOMOPANS-v1 wind noise predictions to measured 50% percentile per wind category (2.5, 5, 7.5, 10, 12.5 and 15 m/s) for different measurement sites of the 2018 JOMOPANS dataset (all data, without ATL processing). Grey areas indicate frequency ranges unlikely to be dominated by wind noise (see Table 1 for details).

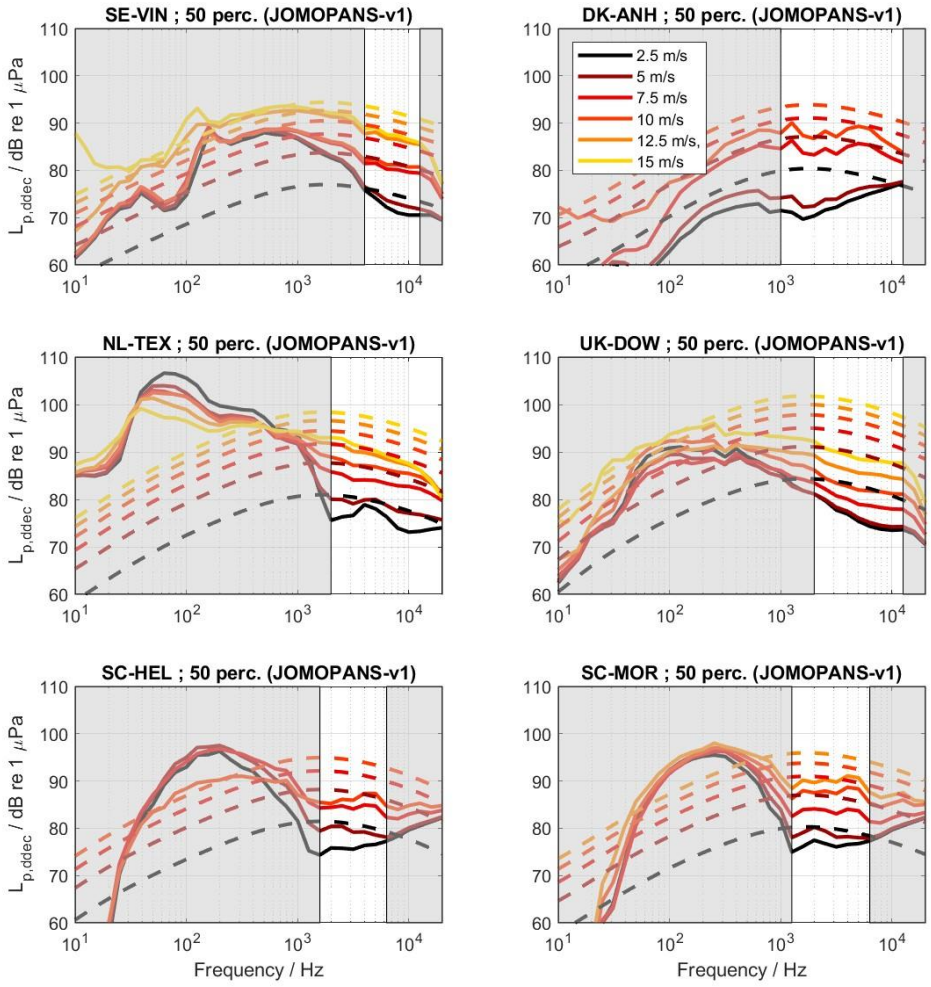

Figure 24 Comparison of JOMOPANS-v1 wind noise predictions to measured 50% percentile per wind category (2.5, 5, 7.5, 10, 12.5 and 15 m/s) for different measurement sites of the 2018 JOMOPANS dataset (ship noise removed using ATL processing). Grey areas indicate frequency ranges unlikely to be dominated by wind noise (see Table 1 for details).

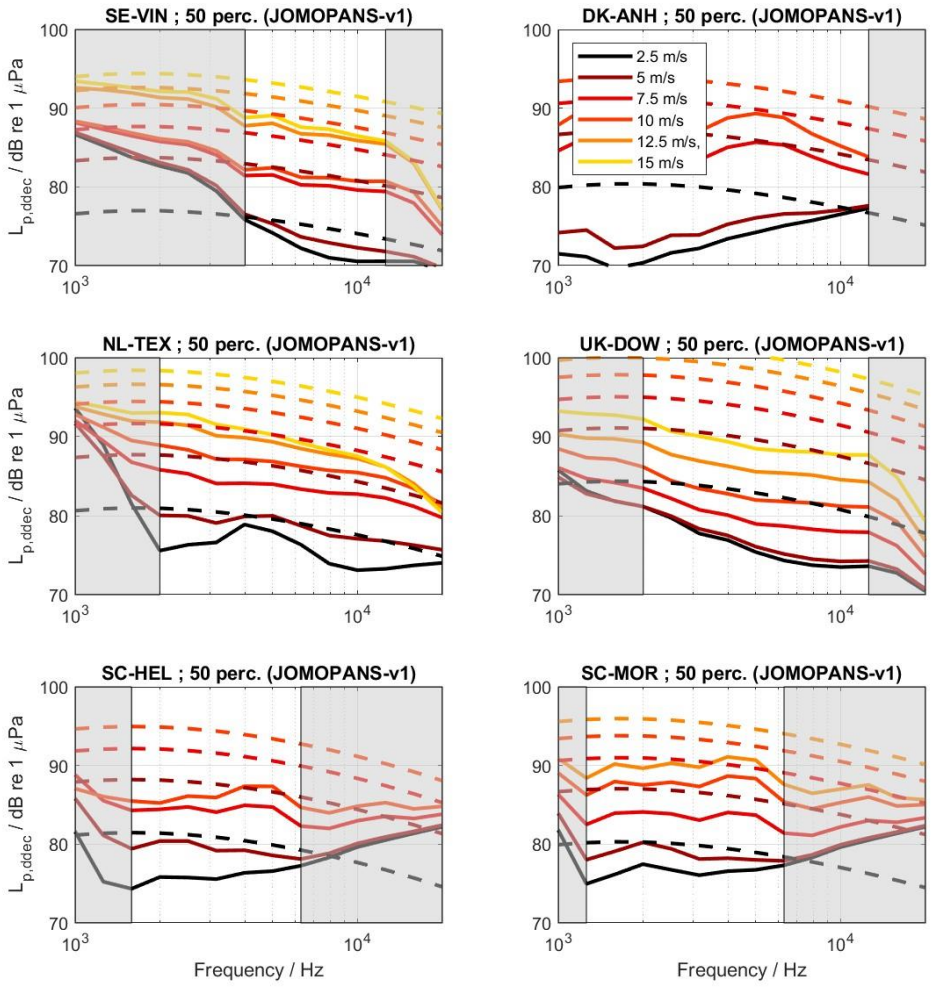

Figure 25 Zoom in on frequency range 1-20 kHz of comparison of JOMOPANS-v1 wind noise predictions to measured 50% percentile per wind category (2.5, 5, 7.5, 10, 12.5 and 15 m/s) for different measurement sites of the 2018 JOMOPANS dataset. Grey areas indicate frequency ranges unlikely to be dominated by wind noise (see Table 1 for details).

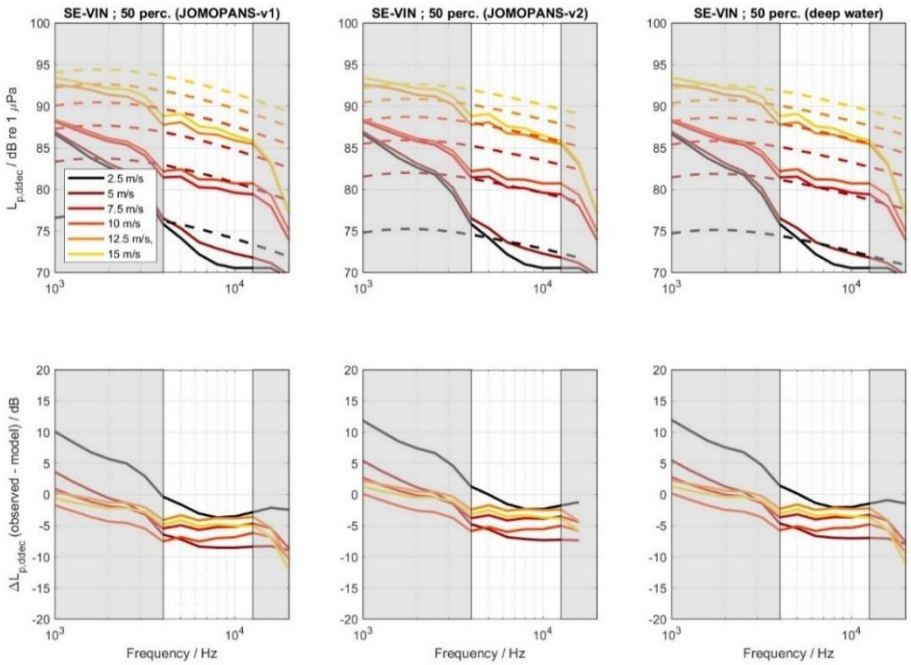

Figure 26 Zoom in on frequency range 1-20 kHz of comparison of JOMOPANS wind noise predictions (v2) to measured 50% percentile per wind category (2.5, 5, 7.5, 10, 12.5 and 15 m/s) for SE-VIN (Site 1). Grey areas indicate frequency ranges unlikely to be dominated by wind noise (see Table 1 for details). The bottom panels show the difference in observed and modelled $L_{p,ddec}$ for each wind speed category.

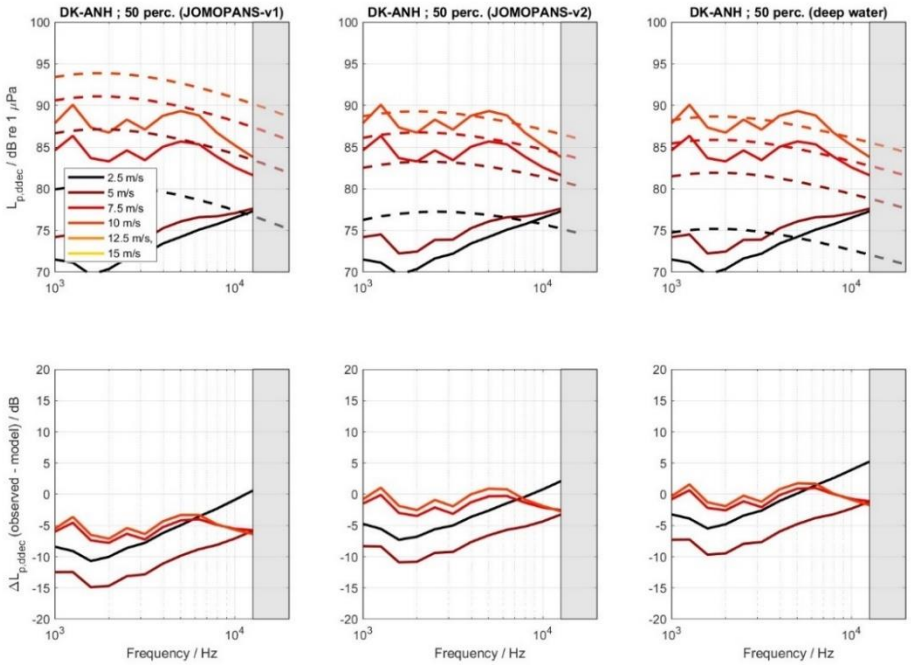

Figure 27 Zoom in on frequency range 1-20 kHz of comparison of JOMOPANS wind noise predictions to measured 50% percentile per wind category (2.5, 5, 7.5, 10, 12.5 and 15 m/s) for DK-ANH (Site 2). Grey areas indicate frequency ranges unlikely to be dominated by wind noise (see Table 1 for details). The bottom panels show the difference in observed and modelled $L_{p,ddec}$ for each wind speed category.

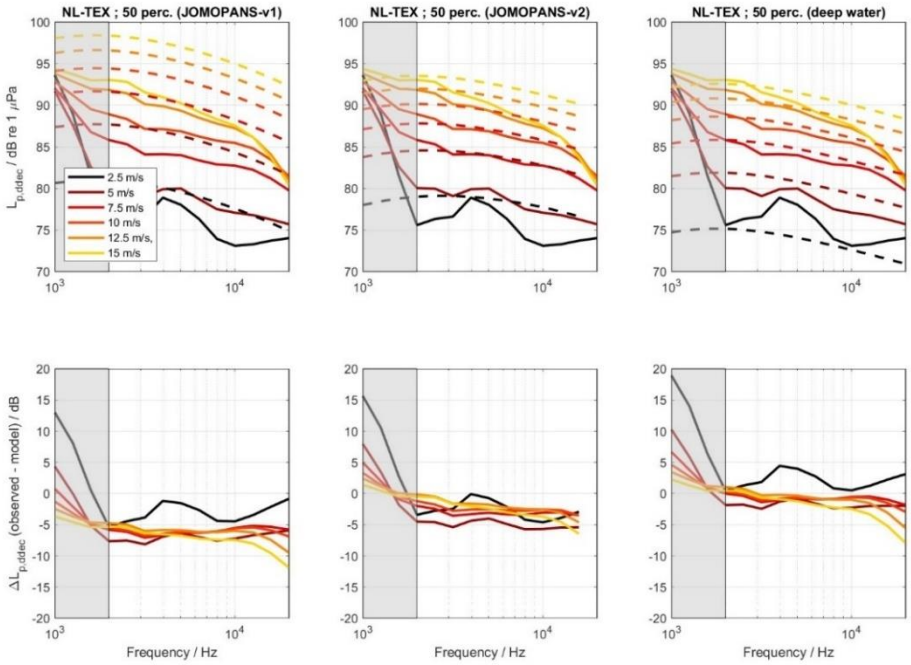

Figure 28 Zoom in on frequency range 1-20 kHz of comparison of JOMOPANS wind noise predictions to measured 50% percentile per wind category (2.5, 5, 7.5, 10, 12.5 and 15 m/s) for NL-TEX (Site 4). Grey areas indicate frequency ranges unlikely to be dominated by wind noise (see Table 1 for details). The bottom panels show the difference in observed and modelled $L_{p,ddec}$ for each wind speed category.

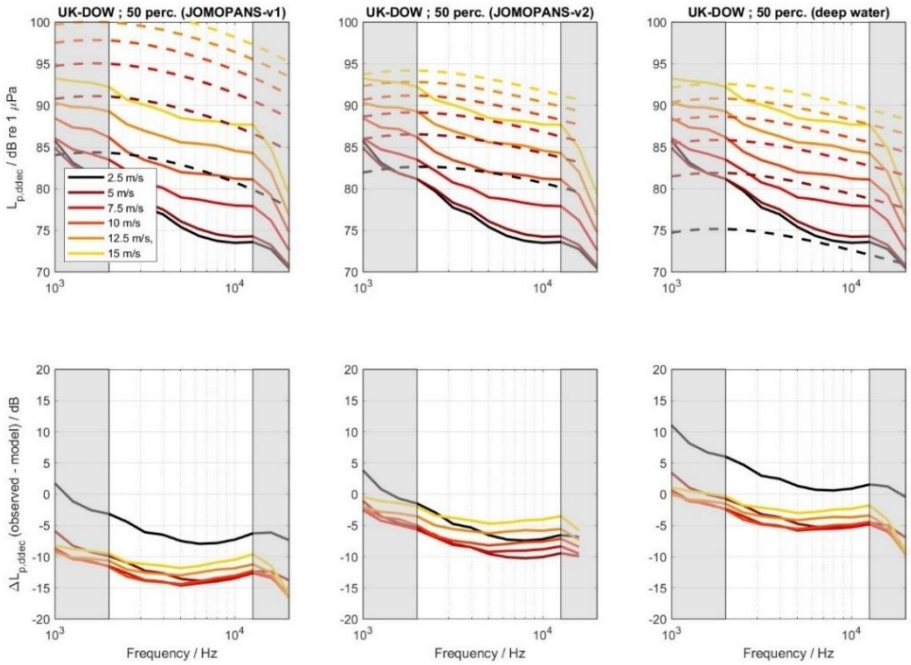

Figure 29 Zoom in on frequency range 1-20 kHz of comparison of JOMOPANS wind noise predictions to measured 50% percentile per wind category (2.5, 5, 7.5, 10, 12.5 and 15 m/s) for UK-DOW (Site 5). Grey areas indicate frequency ranges unlikely to be dominated by wind noise (see Table 1 for details). The bottom panels show the difference in observed and modelled $L_{p,ddec}$ for each wind speed category.

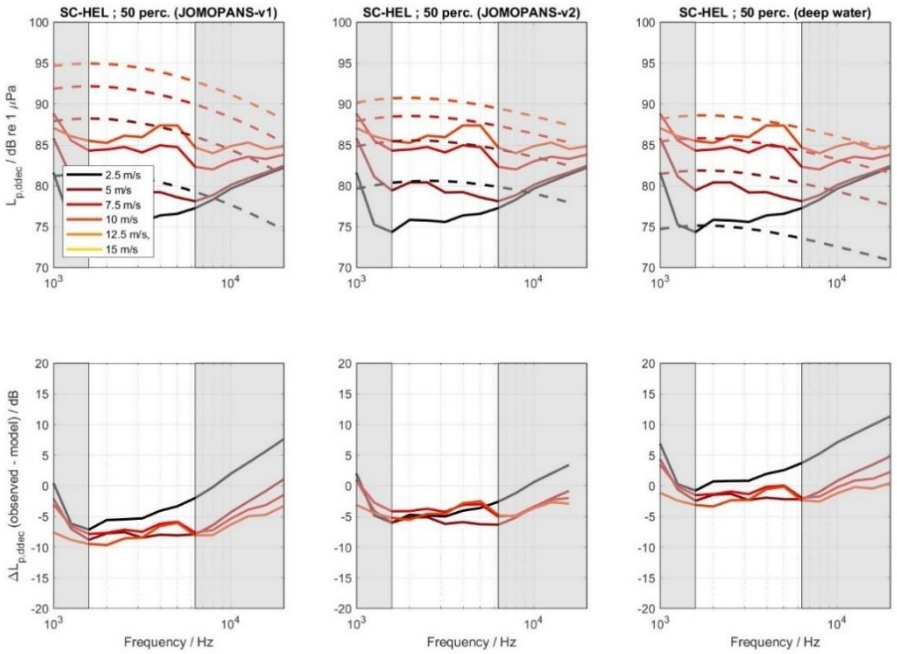

Figure 30 Zoom in on frequency range 1-20 kHz of comparison of JOMOPANS wind noise predictions to measured 50% percentile per wind category (2.5, 5, 7.5, 10, 12.5 and 15 m/s) for SC-HEL (Site 6). Grey areas indicate frequency ranges unlikely to be dominated by wind noise (see Table 1 for details). The bottom panels show the difference in observed and modelled $L_{p,ddec}$ for each wind speed category.

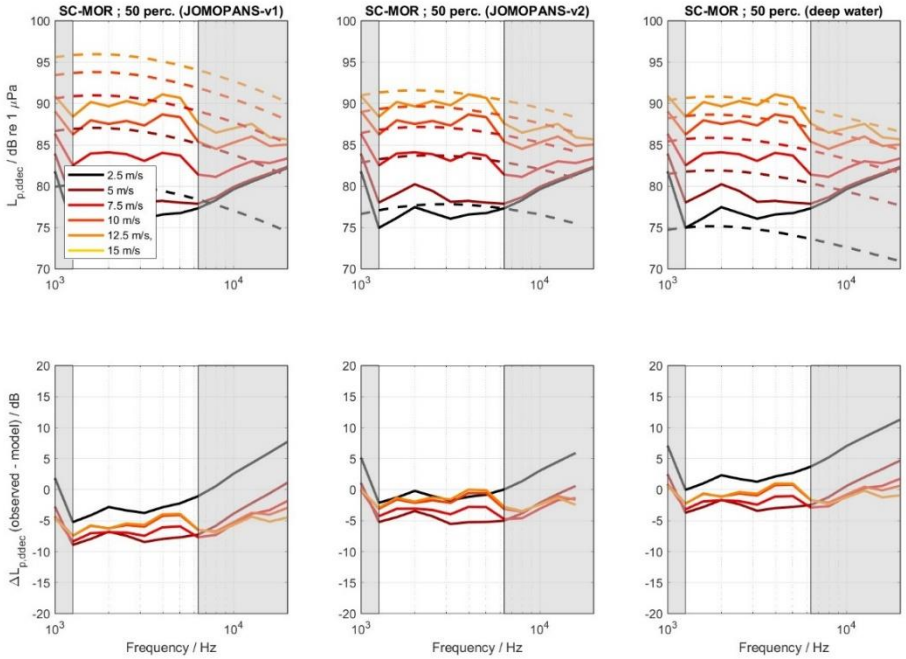

Figure 31 Zoom in on frequency range 1-20 kHz of comparison of JOMOPANS wind noise predictions to measured 50% percentile per wind category (2.5, 5, 7.5, 10, 12.5 and 15 m/s) for SC-MOR (Site 7). Grey areas indicate frequency ranges unlikely to be dominated by wind noise (see Table 1 for details). The bottom panels show the difference in observed and modelled $L_{p,ddec}$ for each wind speed category.

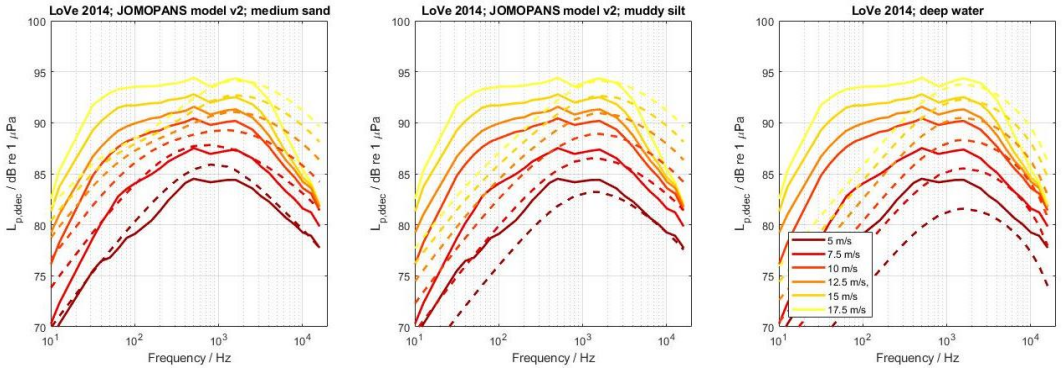

Figure 32 Comparison of different wind noise predictions to measured 50% percentile per wind category (5, 7.5, 10, 12.5, 15 and 17.5 m/s) for the Love 2014 dataset (Site 8).

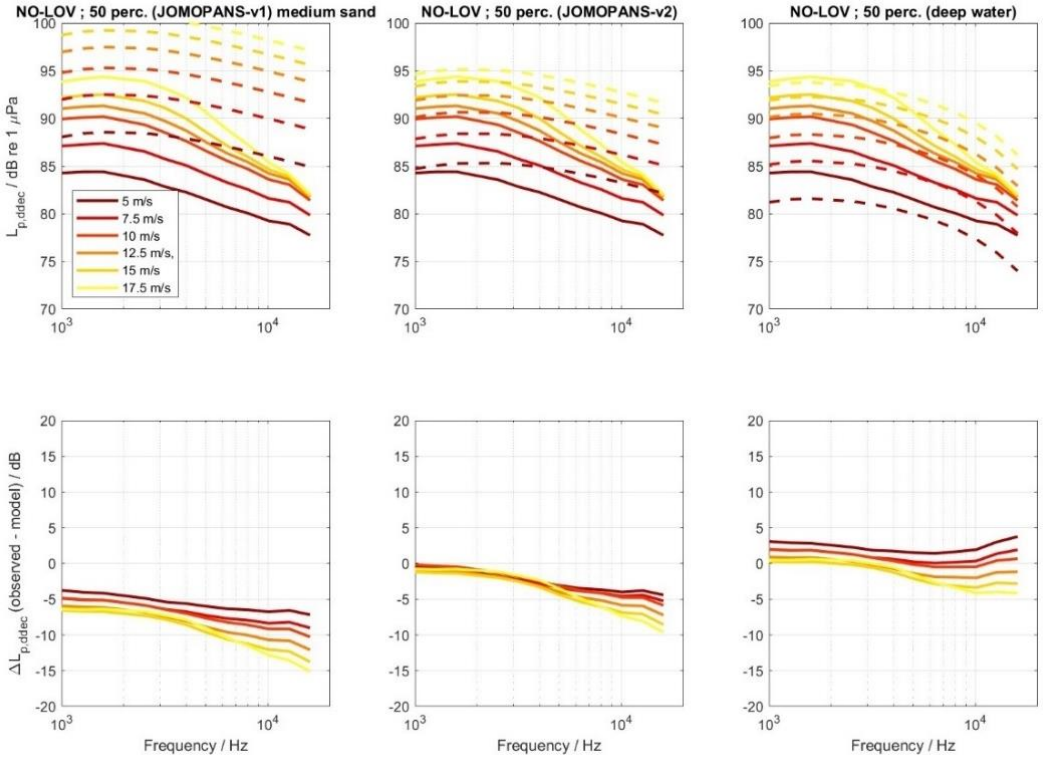

Figure 33 Zoom in on frequency range 1-20 kHz of comparison of JOMOPANS wind noise predictions to measured 50% percentile per wind category (5, 7.5, 10, 12.5, 15 and 17.5 m/s) for the Love2014 dataset (Site 8), assuming a sandy bottom, and a silty bottom. The bottom panels show the difference in observed and modelled $L_{p,ddec}$ for each wind speed category.